Science Advances
AAAS

# Supplementary Materials for

## Structural basis of histone H2A lysine 119 deubiquitination by Polycomb repressive deubiquitinase BAP1/ASXL1

Jonathan F. Thomas *et al.*

Corresponding author: Karim-Jean Armache, karim-jean.armache@nyulangone.org

*Sci. Adv.* **9**, eadg9832 (2023)
DOI: 10.1126/sciadv.adg9832

**This PDF file includes:**

## Figures

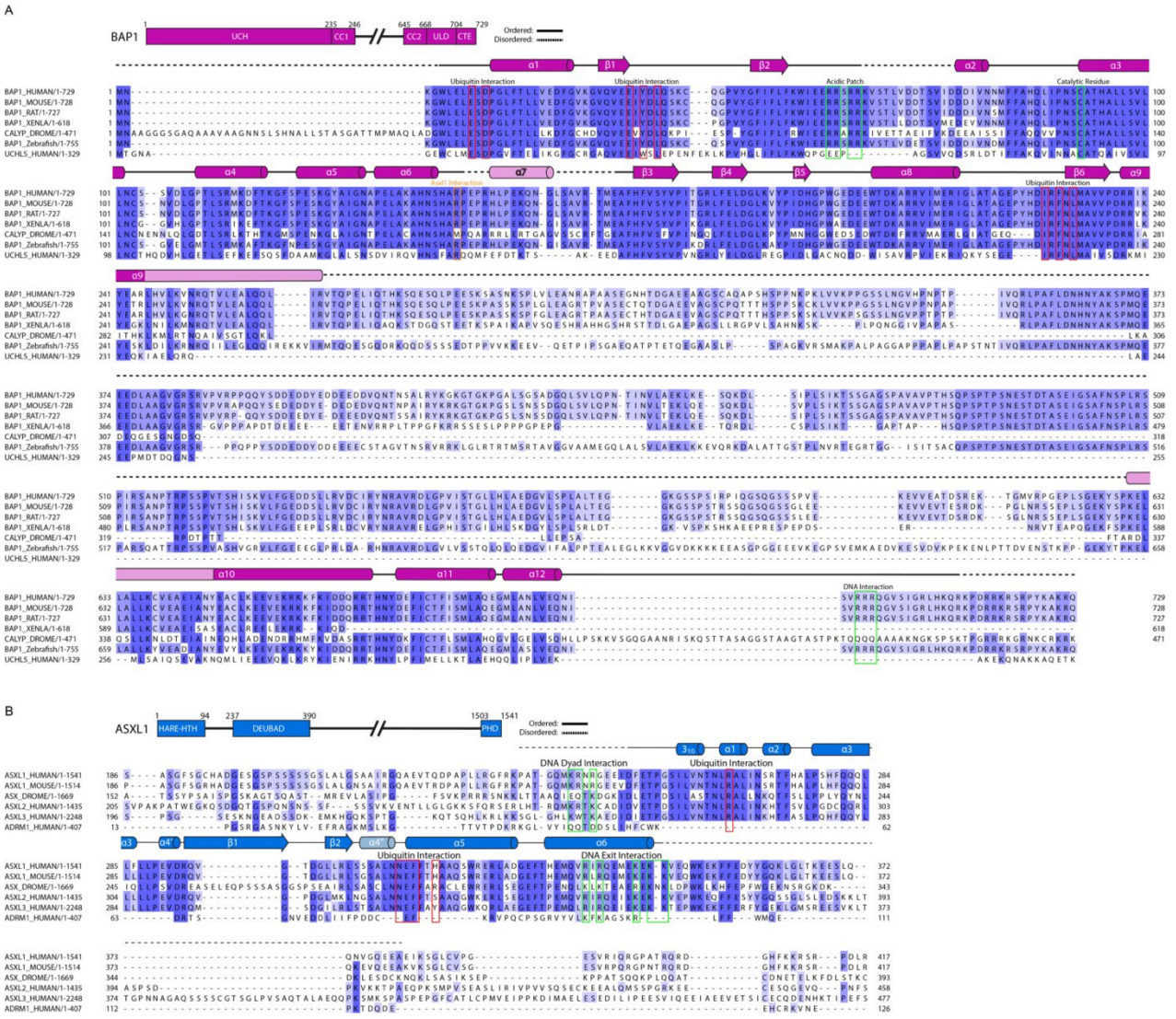


**Fig. S1. BAP1 and ASXL1 sequence alignment.** (A) Protein alignment using MUSCLE to align BAP1, Calypso and UCH-L5 from different organisms. Secondary structure elements modeled in our structure are above sequence alignment. Residues of BAP1 forming the interfaces with Ub, acidic patch, DNA dyad, DNA exit, and the catalytic residue are boxed and labeled. (B) Protein alignment using MUSCLE to align ASXL1 homologs across species (human, mouse, *Drosophila*) and within human cells (ASXL1, ASXL2. ASXL3, RPN13 (ADRM1)). Secondary structure elements in our cryo-EM structure are above sequence alignment. Residues of ASXL1 forming the interfaces with Ub, acidic patch, and DNA exit are boxed and labeled.

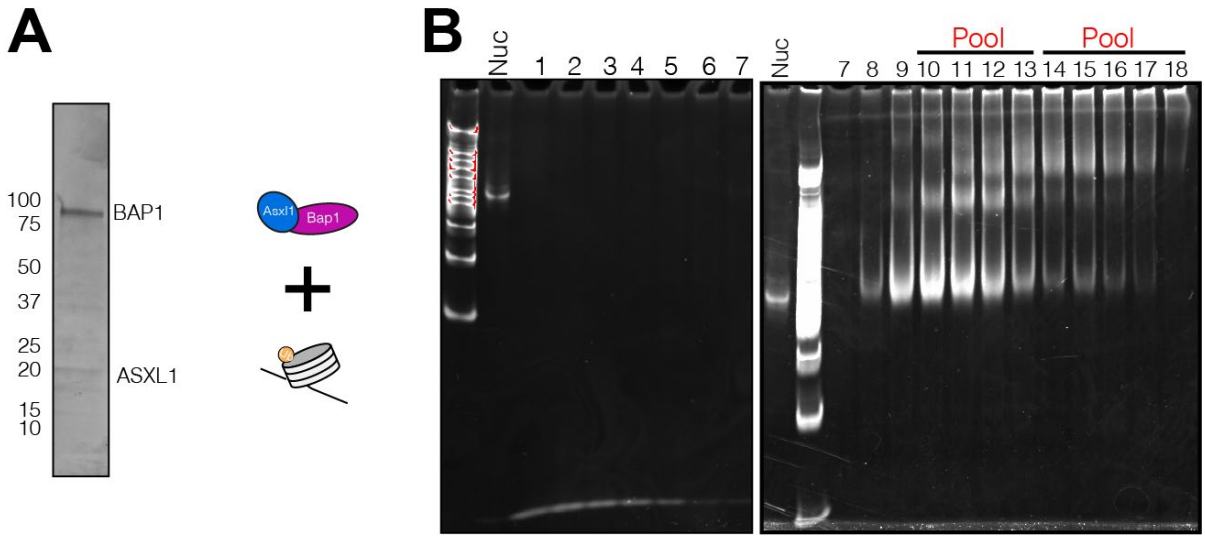


**Fig. S2. BAP1/ASXL1-H2AK119Ub nucleosome sample preparation for structural analysis.** (A) Representative BAP1/ASXL1 complex analyzed by SDS-PAGE (Left). Graphical depiction of BAP1/ASXL1-H2AK119Ub nucleosome assembly (Right). (B) Native PAGE analysis of GraFix fractions from BAP1/ASXL1-H2AK119Ub nucleosome assembly. Gradient fractions pooled and used in Cryo-EM are indicated.

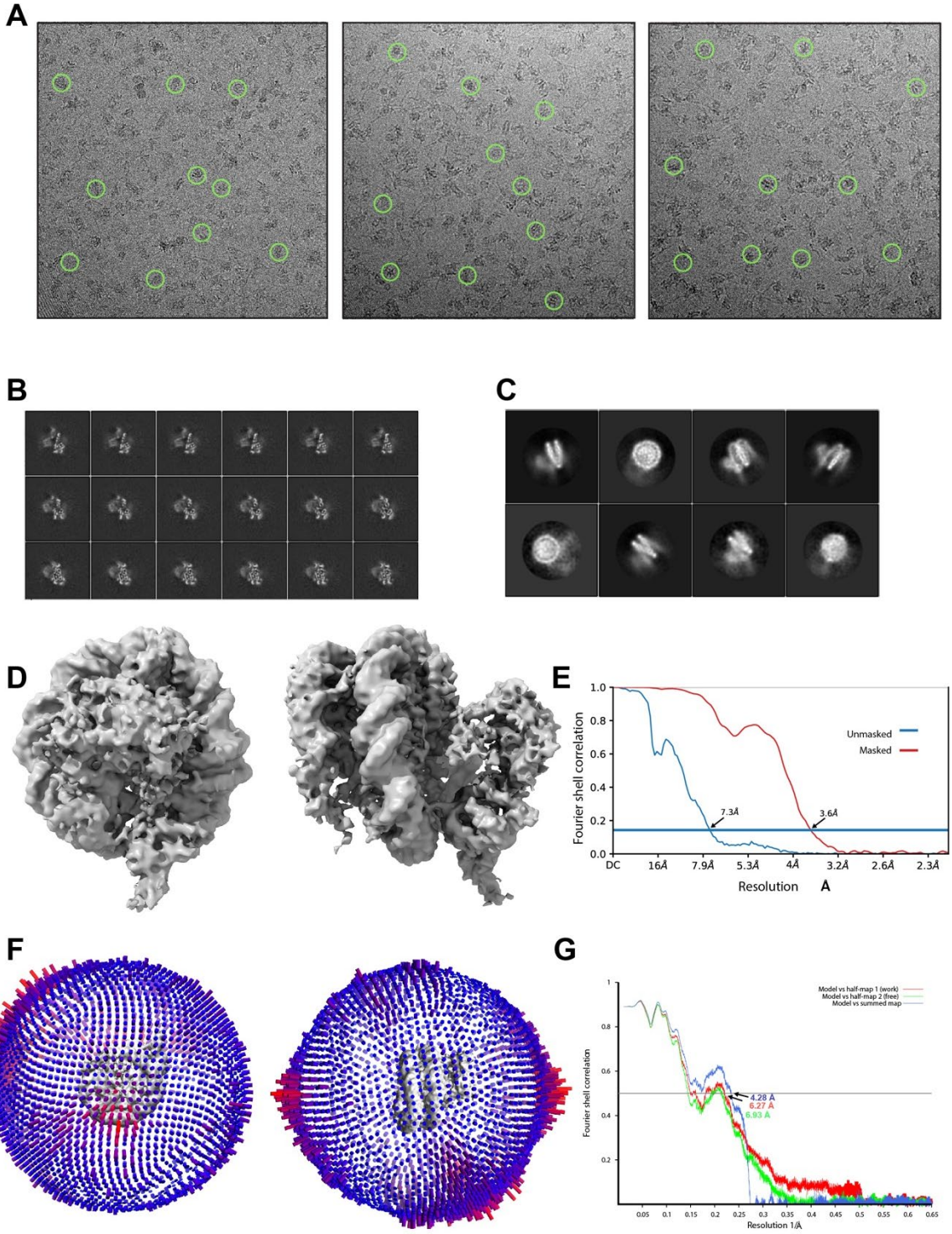


**Fig. S3. Cryo-EM analysis of the BAP1/ASXL1-H2AK119Ub nucleosome complex. (**A) Raw cryo-EM images of BAP1/ASXL1-H2AK119Ub complex were collected as described in Materials and Methods. Representative micrographs from the collection with selected particles of the complex are shown in green circles. (B) Slices at different levels along the Z-axis through the final cryo-EM map. (C) Representative 2D class averages selected from the dataset. (D) Two representative views of the 3D reconstruction of BAP1/ASXL1–H2AK119Ub nucleosome complex. (E) FSC plot of the 3.6 Å BAP1/ASXL1–H2AK119Ub complex between two independently refined half maps (measured at FSC=0.143). (F) Euler angle distribution of assignment of particles used to generate the final 3D reconstruction of the 3.6 Å complex. The

length of every cylinder is proportional to the number of particles assigned to the specific orientation. (G) Cross-validation of the model built against the cryo-EM reconstruction (see Materials and Methods): FSC curves for the model and cryo-EM map calculated from the final model and half map 1 (‘work’, red), half map 2 (‘free’, green) and summed map (blue).

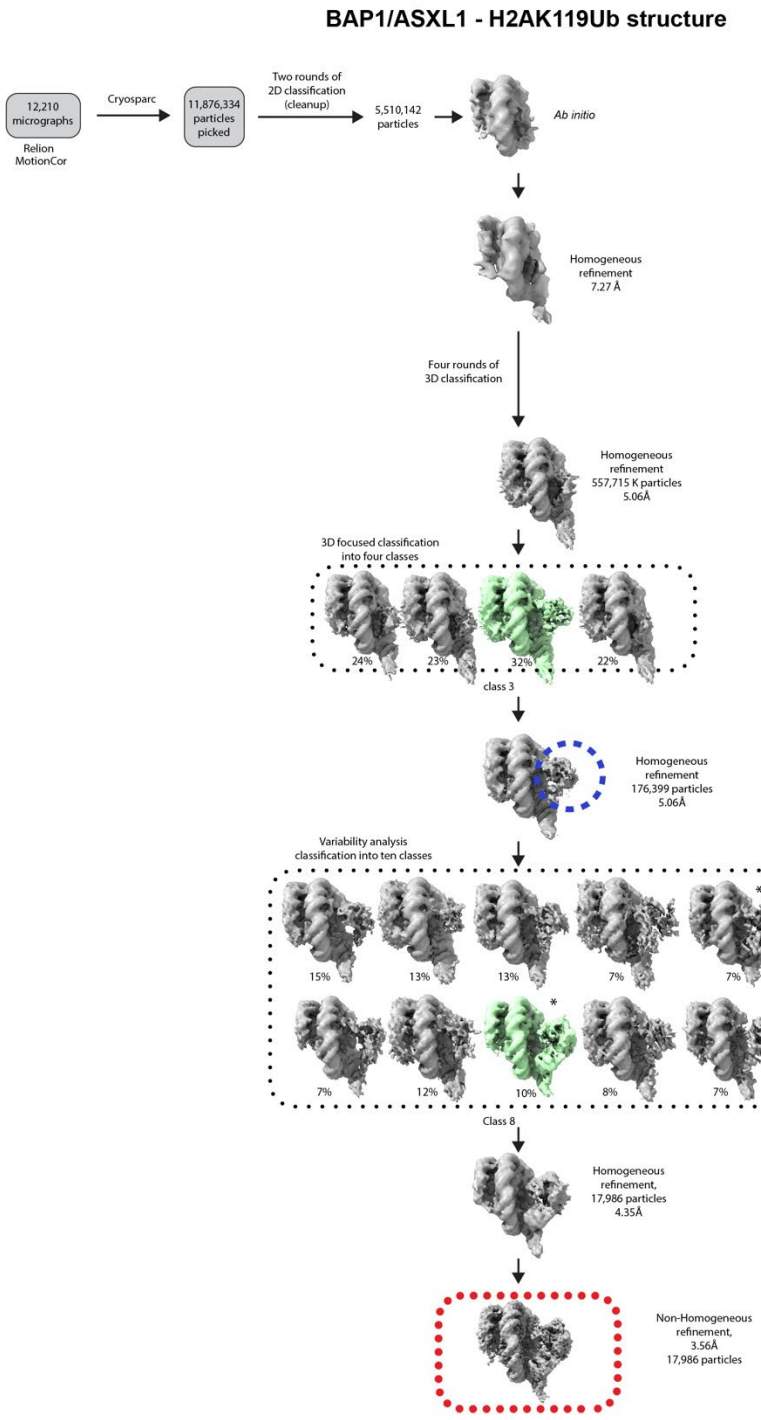


**Fig. S4. 3D classification scheme of BAP1/ASXL1–H2AK119Ub nucleosome samples.** Processing scheme for classification of BAP1/ASXL1-H2AK119Ub nucleosome complex dataset collected on Titan Krios operated at 300 kV. Images represent the path that led to the final subset, with particles and map selected for each step shown in green. A mask applied to BAP1/ASXL1 in 3D focused classification and variability analysis is blue circled. In the variability analysis step, the most stable conformation (classes 5 and 8) is marked (*), with the remaining 3D classes in a more flexible second conformation. Superposition of classes 6 and 8 of the variability analysis step is shown in Fig. S12

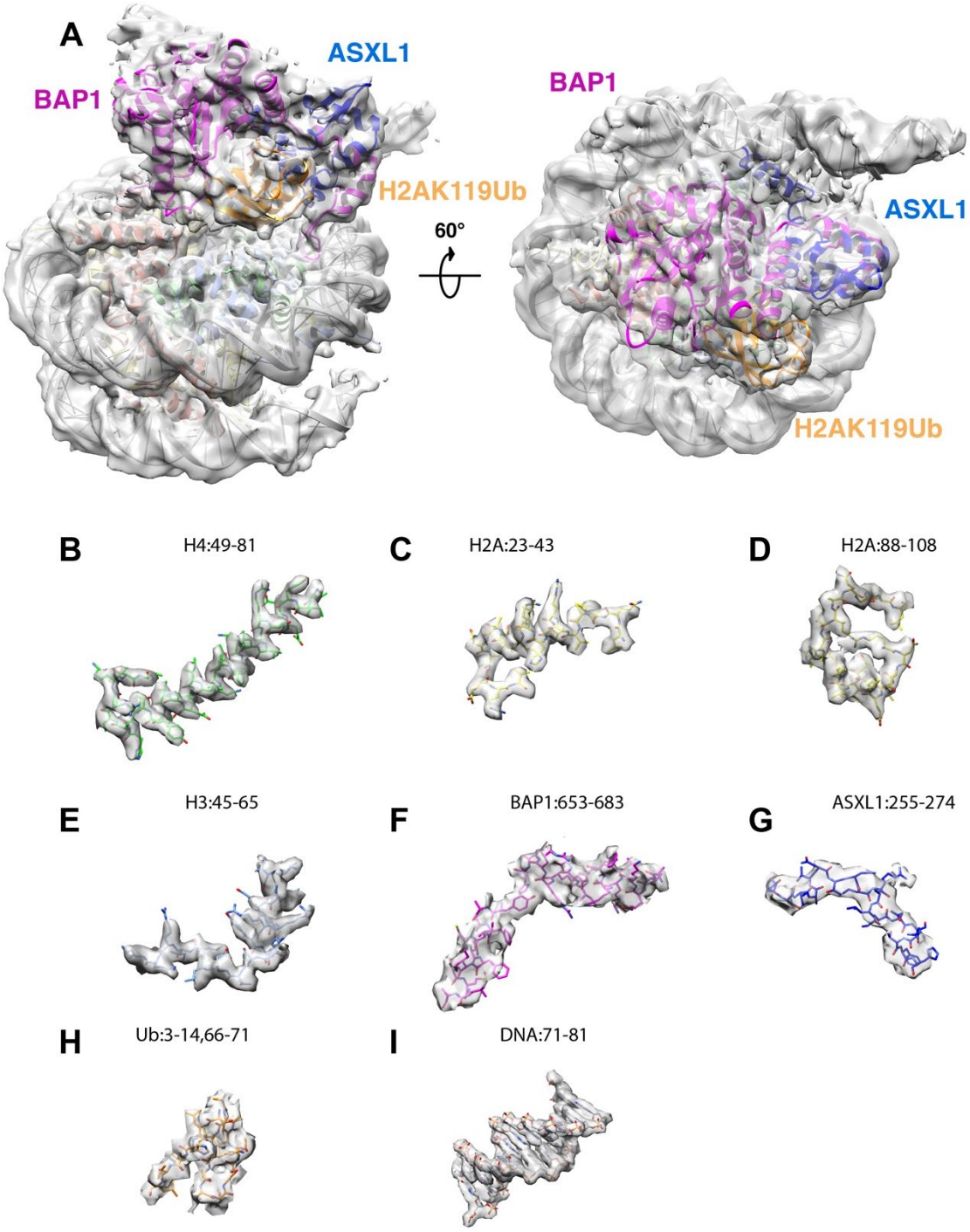


**Fig. S5. Different regions of the cryo-EM map of BAP1/ASXL1-H2A119KUb nucleosome complex.** Selected views of the model fit to the cryo-EM map for the BAP1/ASXL1-H2AK119Ub nucleosome structure are shown. (A) Overview of the complete cryo-EM map/model. (B-I) Selected regions of the model fit to cryo-EM map. A close-up of the model/cryo-EM map fitting in the regions of interaction with the acidic patch and DNA clamp is in Fig. S8. Maps were visualized with Chimera.

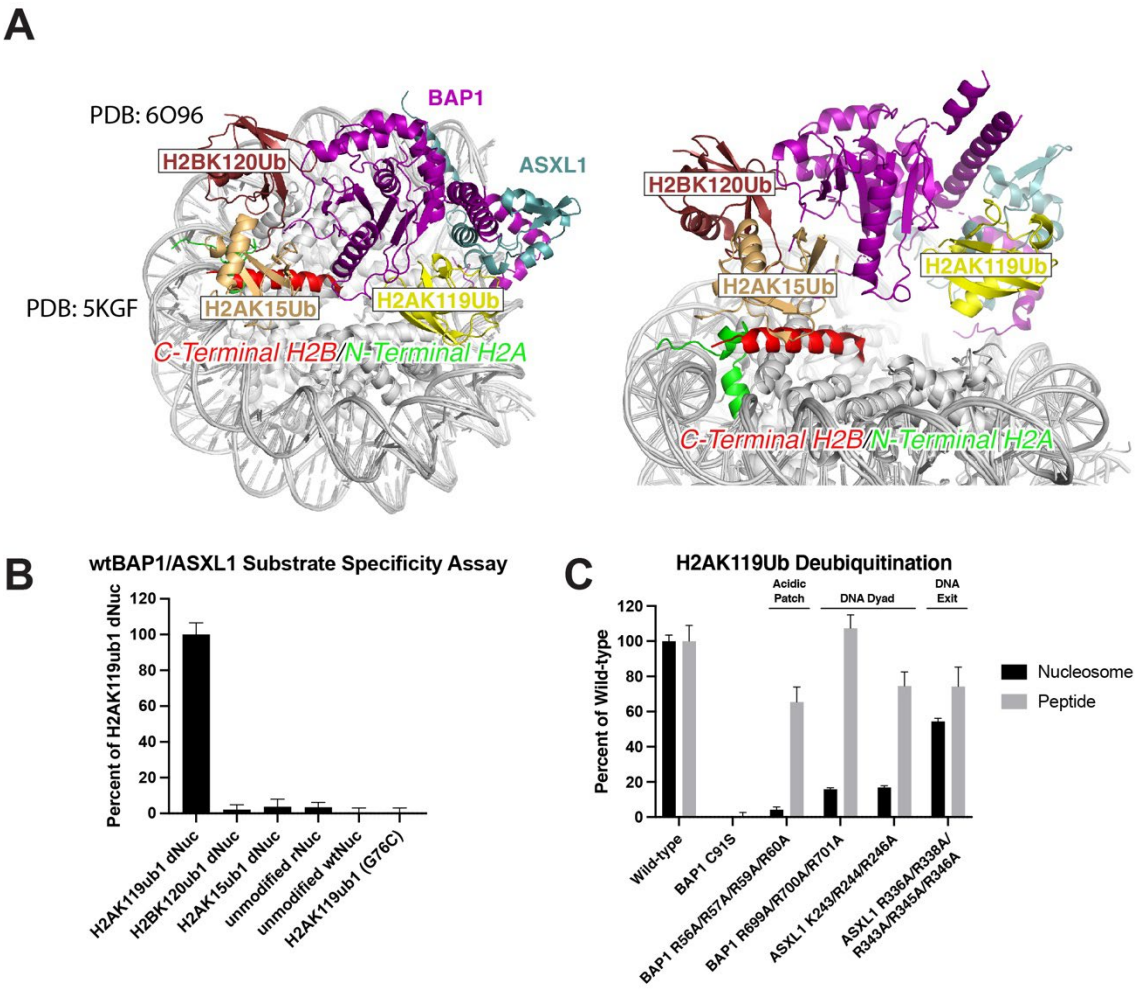


**Fig. S6. Structural alignment and activity assays showing incompatibility of BAP1/ASXL1 with nucleosomal H2BK120Ub and H2AK15Ub.** (A) Our cryo-EM structure was aligned to structures of chromatin modifiers in complex with H2BK120Ub (PDB ID 6o96) (*32*) and H2AK15Ub (PDB 5kgf) (*66*) nucleosomes. The positions of Ub in both complexes are shown in superposition to our BAP1/ASXL1-H2AK119Ub nucleosome complex. H2BK120Ub, H2AK15Ub, and H2AK119Ub are shown and labeled. (B) WT BAP1/ASXL1 dNuc substrate specificity was assessed *in vitro*, comparing H2AK119ub1, H2BK120ub1, H2AK15ub1, unmodified rNuc, unmodified wt nucleosome and crosslinked, nonhydrolyzable nucleosome. BAP1/ASXL1 activity was monitored using the tUI free Ub sensor over 8 minutes at ambient temperature in duplicate (2.5 nM DUB, 10 nM dNuc, 10 nM tUI free Ub sensor) and initial, linear reaction rates are presented as a percentage of H2AK119ub1 (canonical substrate). Free ubiquitin released by BAP1/ASXL1 binds the tUI free Ub sensor, leading to an increase in fluorescence. WT BAP1/ASXL1 is only able to use H2AK119ub1 dNuc as a substrate. C) BAP1/ASXL1 WT and nucleosome interface mutant deubiquitination activity on nucleosomes and peptides are presented as a percentage of wt PR-DUB. Activity was monitored over 11 minutes using the tUI free Ub sensor at ambient temperature in duplicate (5nM DUB, 10 nM dNuc, 10 nM free tUI) or triplicate (16 pM DUB, 10 nM peptide, 10 nM tUI free Ub sensor).

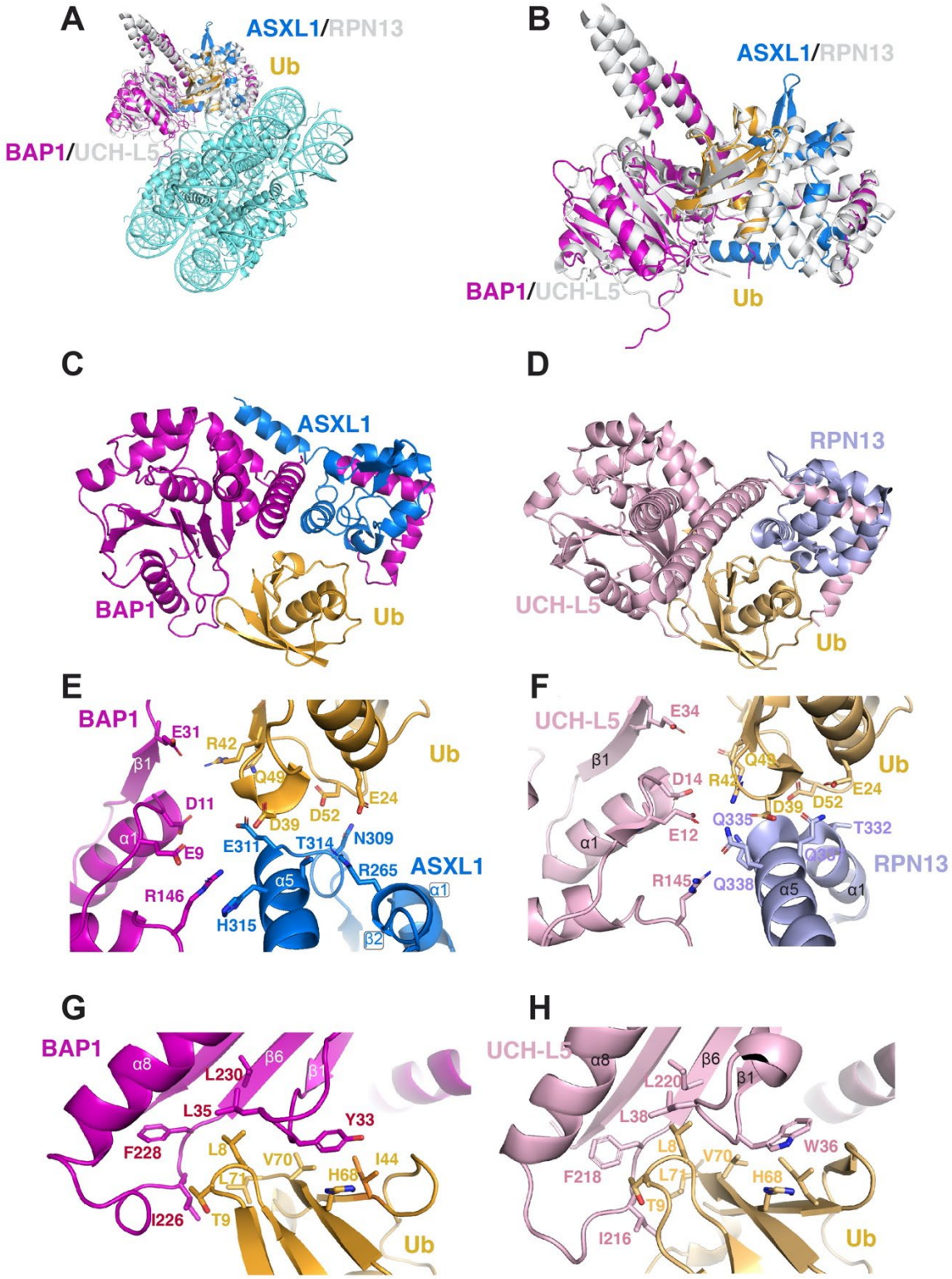


**Fig. S7. The interfaces of BAP1/ASXL1 and UCH-L5/RPN13 with Ub are conserved. (**A) Superposition between BAP1/ASXL1 -H2AK119Ub nucleosome complex determined in this work and UCH-L5/RPN13 (PDB ID 4uel) (*22*). (B) Close up of A showing the Ub interaction of each complex. Side-by-side comparison showing Ub interaction with C) BAP1/ASXL1 and D) UCH-L5/RPN13. Side-by-side comparison of the electrostatic interactions with Ub in the interface of E) ASXL1-BAP1 and F) RPN13-(UCH-L5). Side-by-side comparison of the hydrophobic interactions with Ub in the interface of G) BAP1 and H) UCH-L5. Proteins are color coded as Fig. 2.

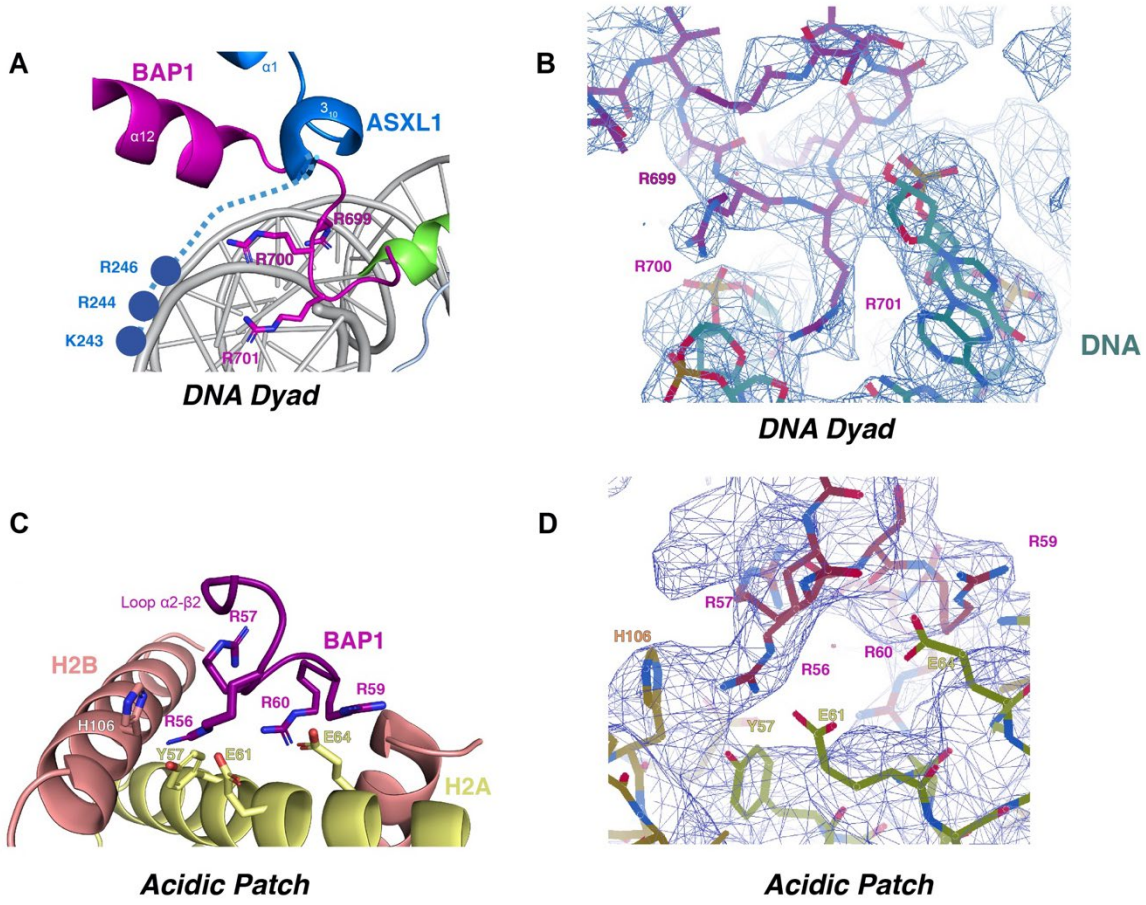


**Fig. S8. Different regions of the cryo-EM map of BAP1/ASXL1-H2A119KUb nucleosome complex.** Selected views of the model fit to the cryo-EM maps for the structure are shown. (A) DNA Clamp model. (B) Map for the region in A (map 3). (C) Acidic patch interface. (D) Map for the region in C (map 2). Maps were visualized with Coot.

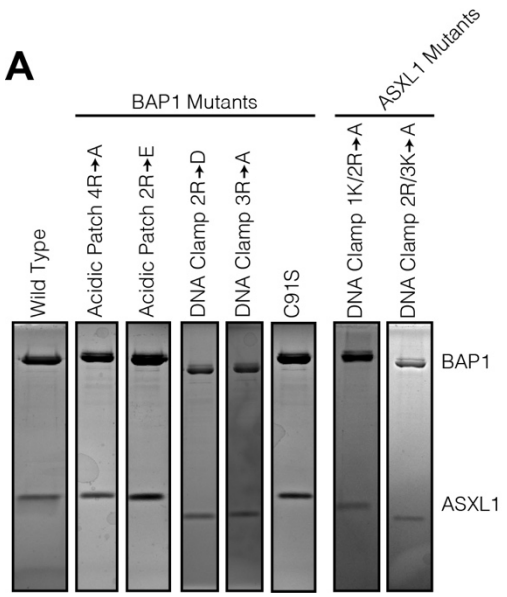


B

| | | Figure Reference | Amino Acid # |
|---|---|---|---|
| BAP1 Mutations | | Acidic Patch 4R→A | 56, 57, 59, 60 |
| | | Acidic Patch 2R→E | 56, 59 |
| | | DNA Clamp 2R→D | 699, 700 |
| | | DNA Clamp 3R→A | 699, 700, 701 |
| | | C91S | |
| ASXL1 Mutations | | DNA Clamp 1K/2R→A | 243, 244, 246 |
| | | DNA Clamp 2R/3K→A | 336, 338, 343, 345, 346 |

**Fig. S9. BAP1/ASXL1 complex assembly for biochemical characterization.**

(A) BAP1/ASXL1 complex analyzed by SDS-PAGE after size exclusion chromatography. (B) Further information regarding BAP1/ASXL1 mutations in panel A.

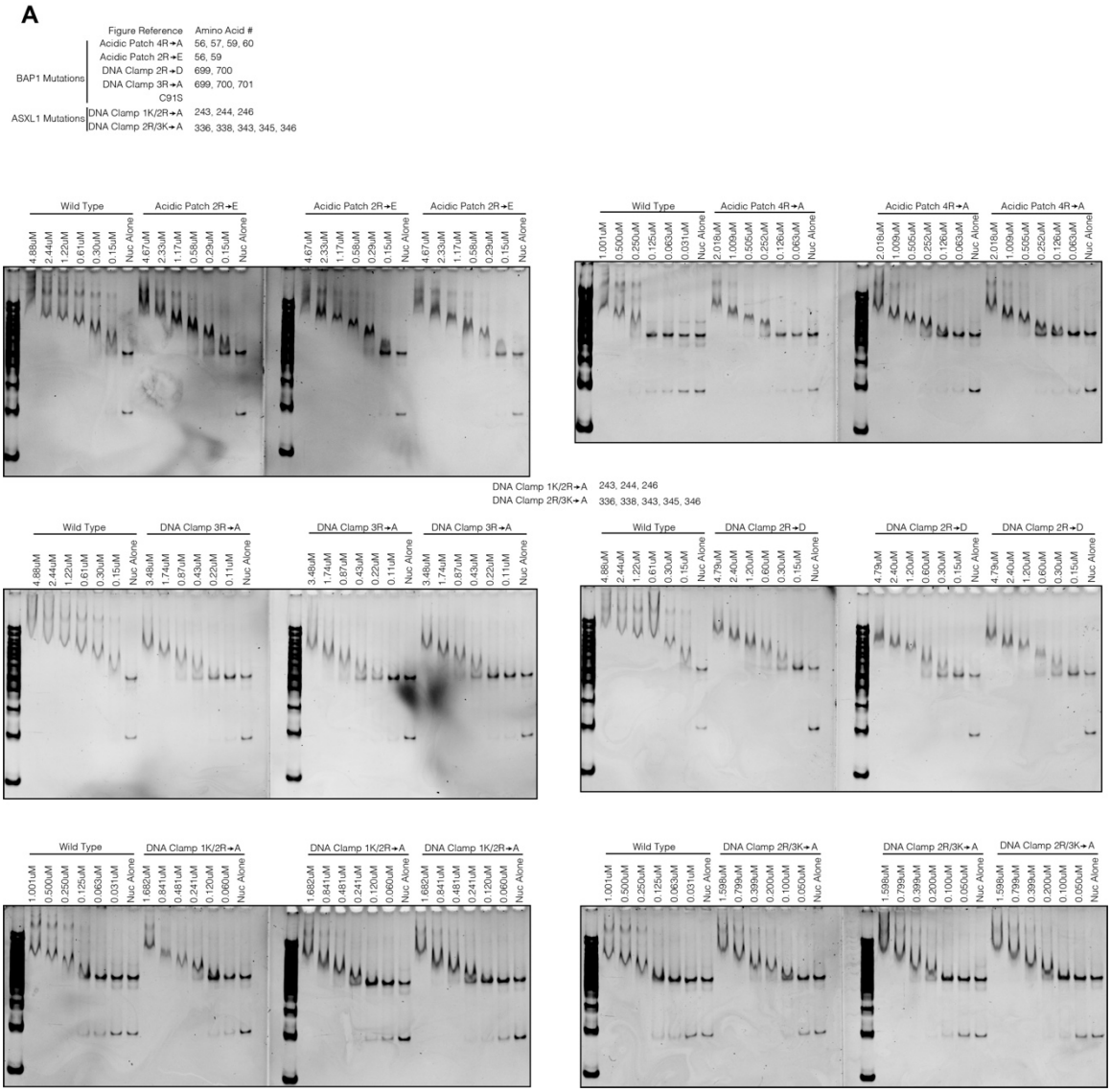


**Fig. S10. Raw data for EMSA of BAP1/ASXL1 mutants.**
(A) Information about BAP1/ASXL1 mutations (top left). Native PAGE of BAP1/ASXL1 bound to H2AK119Ub nucleosomes. BAP1/ASXL1 mutation status and concentration, are marked on gels.

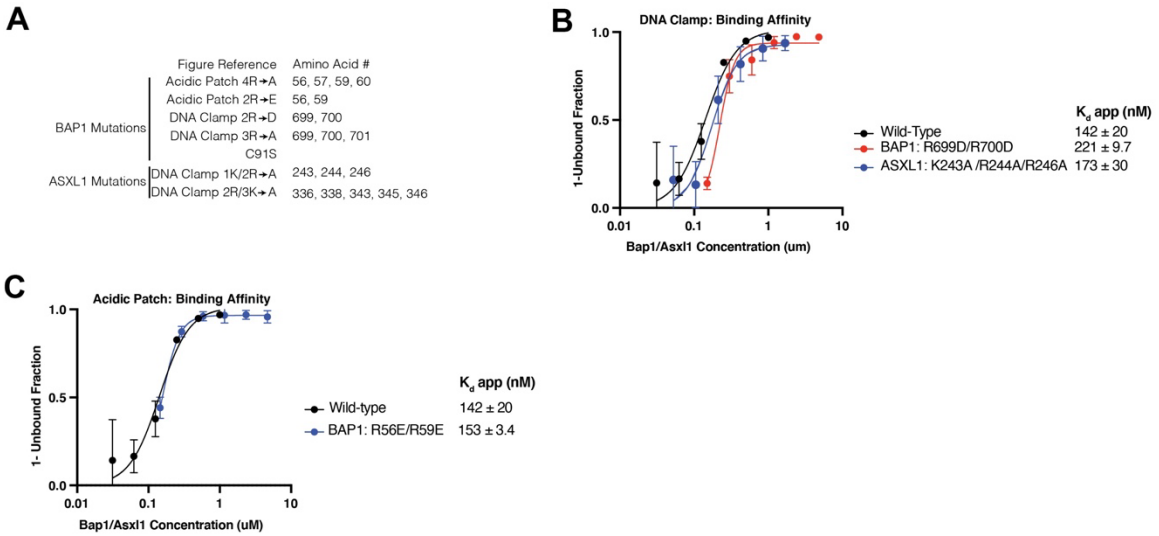


**Fig. S11. Biochemical characterization by EMSA and catalytic activity assay. (**A) Summary of information of BAP1/ASXL1 mutations is shown. (B-C) Nucleosome binding curves (by EMSA) for the DNA clamp mutants (B) and BAP1 acidic patch interaction mutant C). Each data point and error bar indicate the mean ± SD from three independent experiments. The standard errors of dissociation constants (Kd) are indicated.

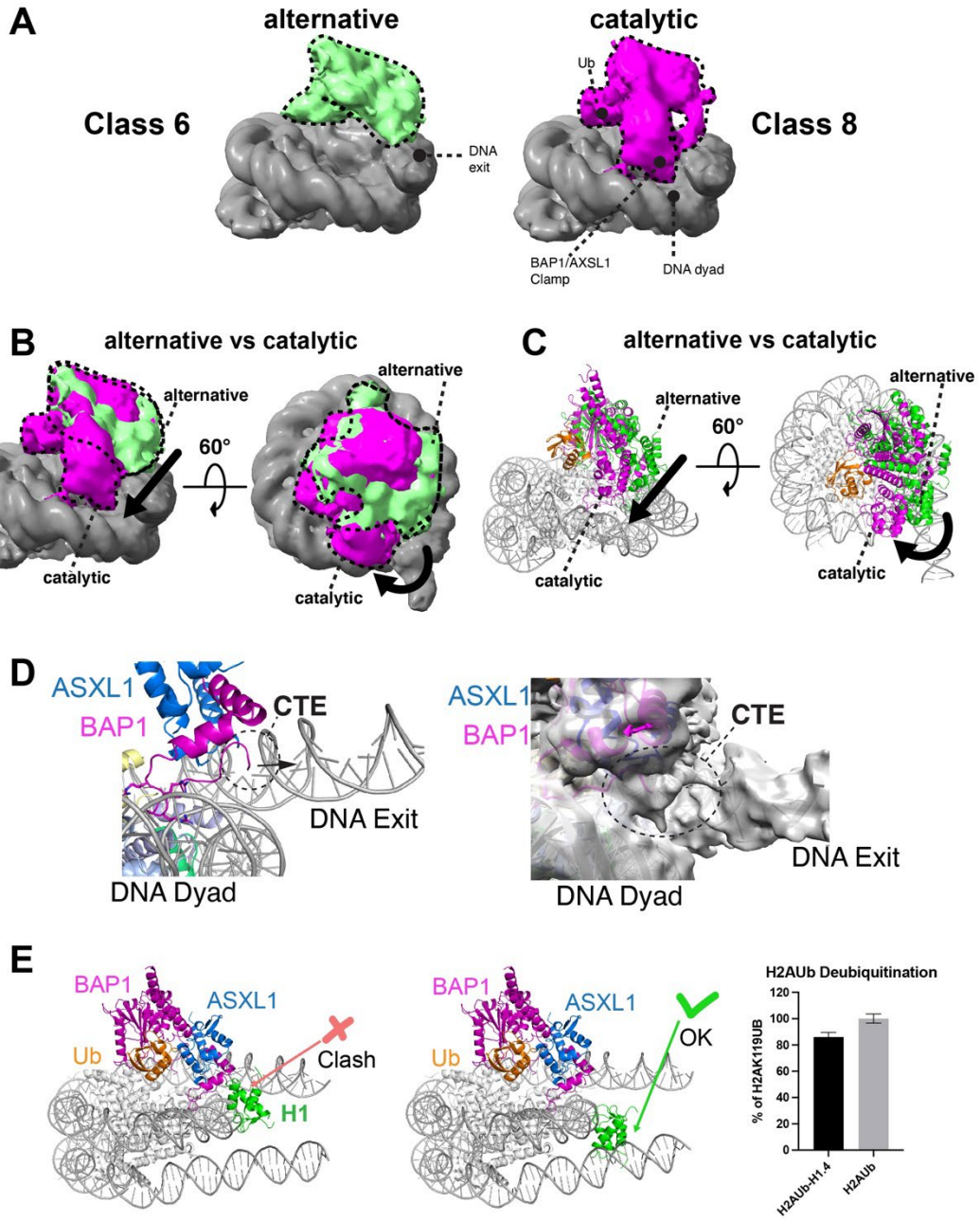


**Fig. S12. Conformations of BAP1/ASXL1 on the nucleosome.** (A) Two different cryo-EM maps from variability analysis (shown in Fig. S4) depicting an alternative, more flexible conformation in class 6 (left) compared with the more stable conformation of BAP1/ASXL1-H2AK119Ub nucleosome in class 8 (right). (B) Superposition of both classes. (C) Model from superposition in (B). The more stable conformation is characterized by the binding of the BAP1/ASXL1 clamp near the DNA dyad. BAP1/ASXL1 clamp might bind to the DNA exit rather than the DNA dyad in the more flexible conformation. Maps filtered with Gaussian filter at 2.5 SD. (D) BAP1 CTE region observed in our structure shown in the model (left) and the fitting to an unsharpened (map 1). (E) Superposition of H1 in the structure of BAP1/ASXL1-H2AK119Ub nucleosome determined in this study, with the structure of the chromatosome (PDB ID 7pfv) (*44*), showing the (left) incompatibility between linker histone H1.4 (when it is bound to DNA at the side of BAP1/ASXL1) and BAP1/ASXL1 clamp at the dyad axis, also near the usual conformation of the H2A docking domain; and (middle) the compatibility of BAP1/ASXL1 when H1.4 is bound on the other side of the DNA linker. (F) BAP1/ASXL1 deubiquitination activity on H2AK119Ub-187bp nucleosome and H2AK119Ub-187bp chromatosome (right).

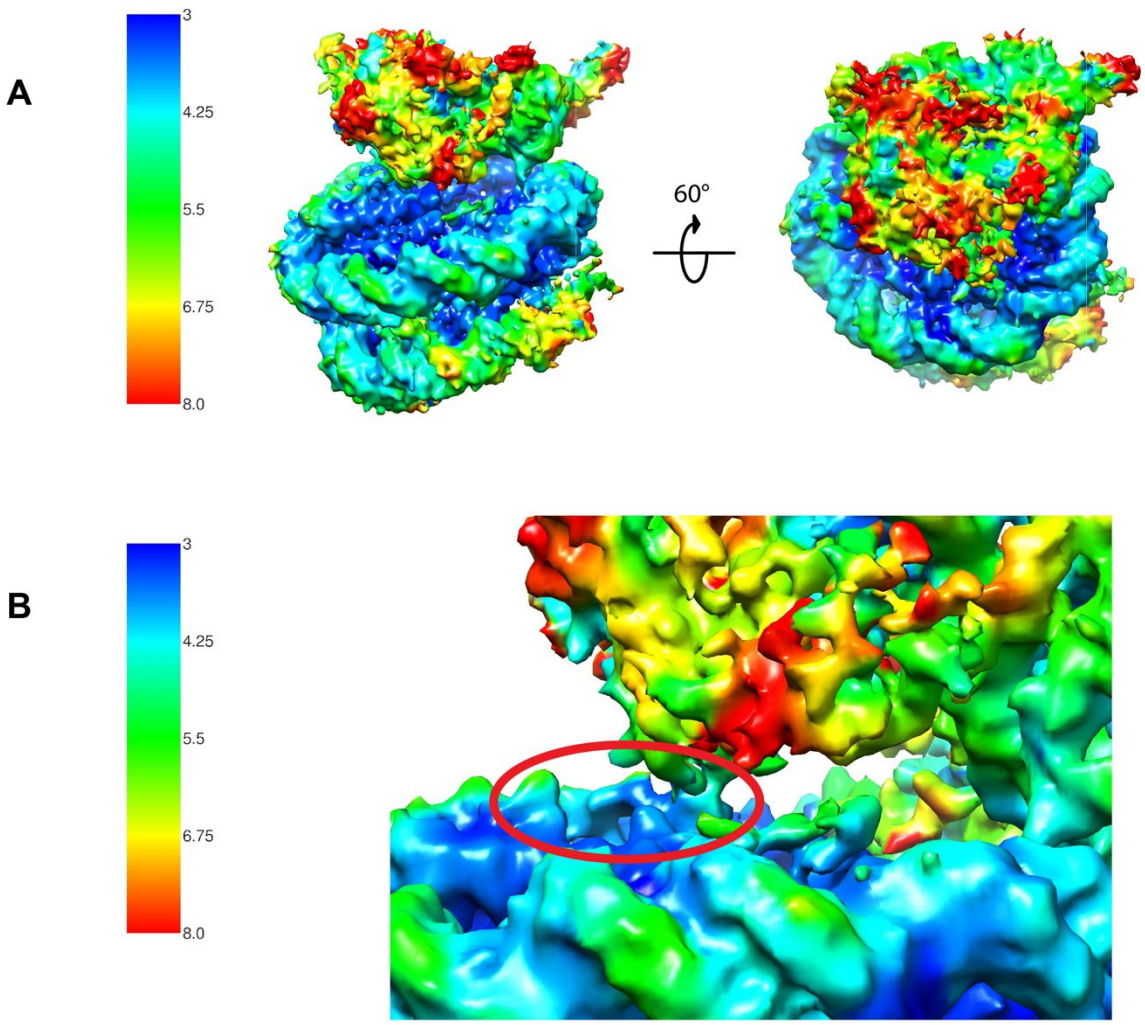


**Fig. S13. Local resolution heat map for the reconstruction for BAP1/ASXL1-H2AK119Ub nucleosome complex.** (A) Local resolution heat map (of map 1), calculated using cryoSPARC's built-in local resolution algorithms. Front view of the Coulomb potential maps visualized in Chimera. (B) Close-up of the R-finger region of BAP1 interacting with the acidic patch. The model fit to the cryo-EM map in this region is shown in Fig S8.

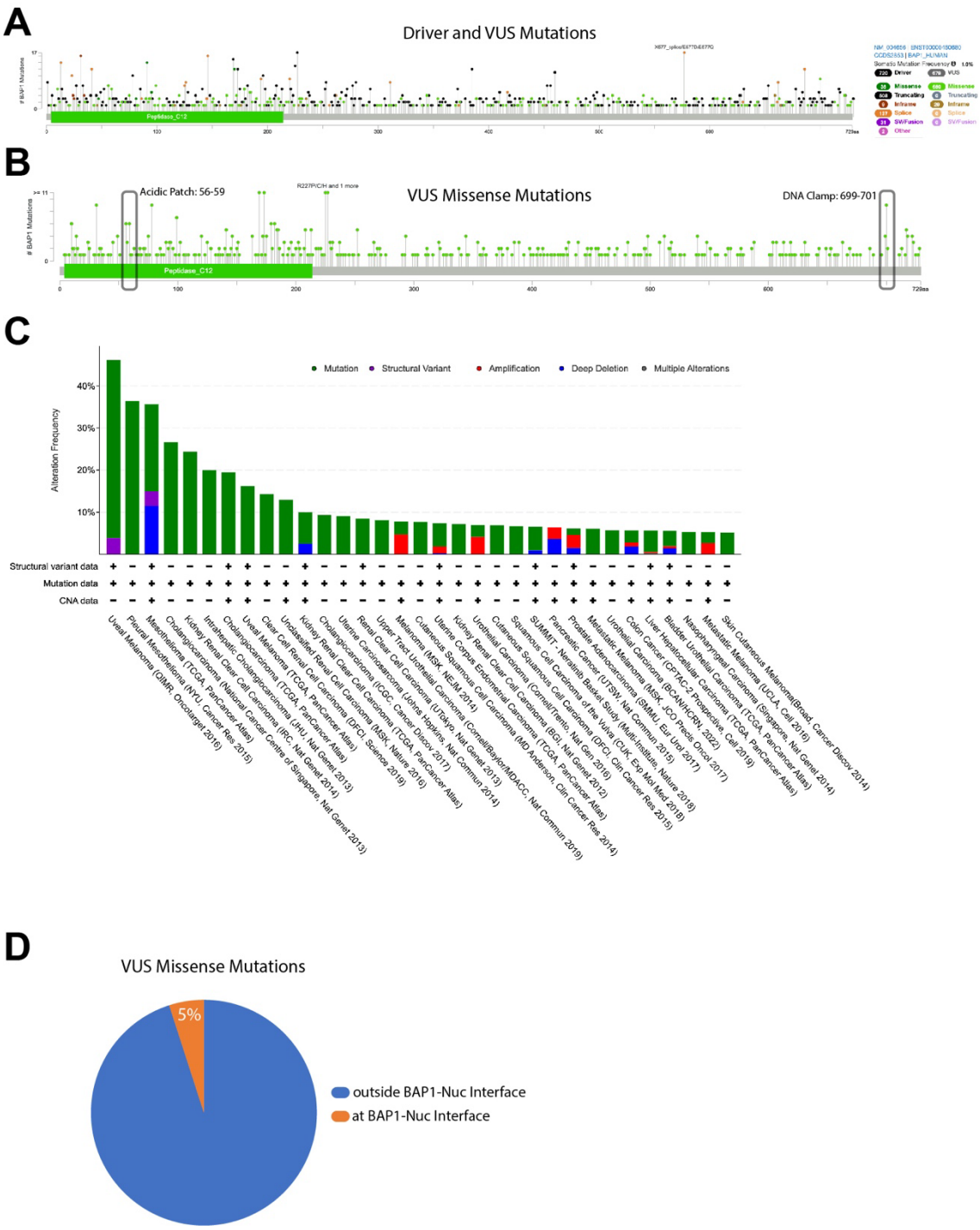


**Fig. S14. BAP1 mutations found in cancer.** cBioPortal database was searched for a curated set of non-redundant cancer studies on BAP1 (*67, 68*). (A-B) Driver and VUS mutations mapped across the amino acid sequence of BAP1 with mutational frequency represented by height. (C) BAP1 cancer associated mutations compared with alteration frequency and associated disease. (D) Pie chart representation of the total number of VUS mutations and the number of VUS mutations at BAP1-Nucleosome interfaces.

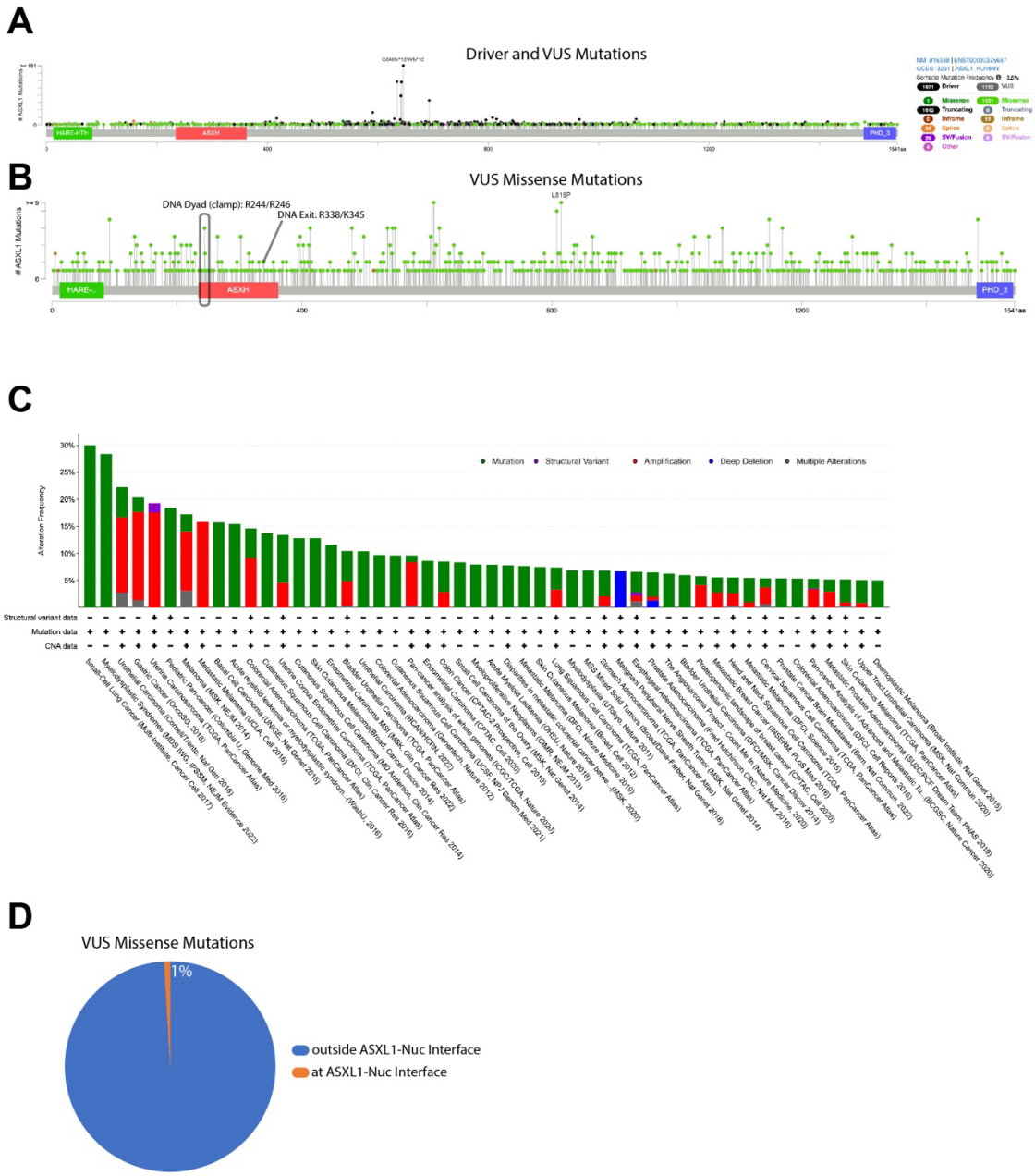


**Fig. S15. ASXL1 mutations found in cancer.** cBioPortal database was searched for a curated set of non-redundant cancer studies on ASXL1 (*67, 68*). (A-B) Driver and VUS mutations mapped across the amino acid sequence of ASXL1 with mutational frequency represented by height. (C) ASXL1 cancer associated mutations compared with alteration frequency and associated disease. (D) Pie chart representation of the total number of VUS mutations and the number of VUS mutations at BAP1-Nucleosome interfaces.

**Table S1. Summary for cryo-EM data collection, refinement and deposition**

| **Dataset** | **BAP1/ASXL1-H2AK119Ub** | |
|---|---|---|
| Microscope | Titan Krios | |
| Voltage (kV) | 300 | |
| Camera | K3 Summit (Gatan) | |
| Magnification | 105,000 | |
| Pixel size (Å) | 0.825 (0.4125) | |
| Defocus range (μm) | -0.9 : -1.9 (-1.44) | |
| Number of images | 12,210 | |
| Total electron dose (e-/Å2) | 57.12 | |
| Number of frames | 50 | |
| Initial number of particles | 11,876,334 | |
| Particles selected after 2D cleanup | 5,510,142 | |
| Particles in final reconstruction Map 1 | 17,986 | |
| Particles in final reconstruction Map 2 | 20,559 | |
| Particles in final reconstruction Map 3 | 39,056 | |
| | | |
| **PDB**<br>-BAP1/ASXL1-H2A119Ub nuc | | PDB 8SVF |
| | Resolution | |
| **Map 1:** Used to build the overall structure<br>EMDB 3.6 Å BAP1/ASXL1- H2AK119Ub nuc | 3.6 Å | EMD-40791 |
| **Map 2:** Used for acidic patch interactions<br>EMDB 3.2 Å BAP1/ASXL1- H2AK119Ub nuc | 3.2 Å | EMD-40790 |
| **Map 3:** Used for DNA clamp interactions<br>EMDB 3.2 Å BAP1/ASXL1- H2AK119Ub nuc | 3.2 Å | EMD-40789 |

**Table S2. Summary for Cryo-EM data collection, refinement and validation statistics**

| | BAP1/ASXL1-H2A119Ub nucleosome (EMD-40789) (PDB 8SVF) |
|---|---|
| **Data collection and processing** | |
| Magnification | 105,000x |
| Voltage (kV) | 300 |
| Electron exposure (e–/Å$^2$) | 57.12 |
| Defocus range (μm) | -0.9 to -1.9 (-1.44) |
| Pixel size (Å) | 0.825 (0.4125) |
| Symmetry imposed | *C1* |
| Initial particle images (no.) | 11,876,334 |
| Final particle images (no.) | 39,056 |
| Map resolution (Å) | 3.2 |
| 0. 143 FSC threshold | |
| Map resolution range (Å) | 3.2-149.6 |
| | |
| **Refinement** | |
| Initial model used (PDB code) | 3tu4, 6hgc, 4uel, 7k5y AlphaFold Multimer |
| Model resolution (Å) | 3.2 |
| FSC threshold (0.143) | |
| Model resolution range (Å) | 3.2-149.6 |
| Map sharpening *B* factor (Å$^2$) | -5 |
| Model composition | |
| Non-hydrogen atoms | 15,301 |
| Protein residues | 1,195 |
| Nucleotides | 295 |
| *B* factors (Å$^2$) | |
| Protein | 181.09 |
| Nucleotides | 168.01 |
| R.m.s. deviations | |
| Bond lengths (Å) | 0.008 |
| Bond angles (°) | 0.870 |
| Validation | |
| MolProbity score | 1.77 |
| Clashscore | 8.52 |
| Poor rotamers (%) | 2.45 |
| Ramachandran plot | |
| Favored (%) | 97.94 |
| Allowed (%) | 2.06 |
| Disallowed (%) | 0.0 |

**Supplementary Table S3. Catalytic Activity Model Fit and Results.**
Average of three independent catalytic experiments for PR-DUB WT and nucleosome interface mutants and P value for fit model selection. For each mutant the Michaelis-Menten and allosteric sigmoidal models were compared using an F-test. The allosteric sigmoidal model was the best model (P value <0.5) for all mutants except the DNA dyad mutant, BAP1 R699A/R700A/R701A. For this mutant, results for both fits are shown.

| Mutation | Interaction Site | $k_{cat}/K_{0.5}$ ± SD ($s^{-1}*M^{-1}$) | $K_{0.5}$ ± SD (nM) | $k_{cat}$ ± SD (sec-1) | h ± SD (Hill Coef.) | Fit Model P Value |
|---|---|---|---|---|---|---|
| **Wild-type** | | 1.9E+06 ± 4.1E-01 | 166 ± 29 | 0.31 ± 0.04 | 1.7 ± 0.2 | <0.0001 |
| **BAP1 R699A/R700A/R701A** | DNA Dyad | <9.3E+05 | >300 | 0.28 ± 0.87 | 0.9 ± 0.1 | 0.4864 |
| | | <7.0E+05 | >300* | 0.21 ± 0.04* | NA** | |
| **ASXL1 K243/R244/R246A** | DNA Dyad | 5.1E+05 ± 1.3E-01 | 167 ± 35 | 0.085 ± 0.012 | 1.6 ± 0.2 | 0.0015 |
| **BAP1 R56A/R57A/R59A/R60A** | Acid Patch | 1.1E+05 ± 2.8E-02 | 156 ± 35 | 0.017 ± 0.002 | 1.4 ± 0.2 | 0.0113 |
| **ASXL1 R336A/R338A/K343A/K345A/K346A** | DNA Exit | 7.1E+05 ± 1.6E-01 | 124 ± 24 | 0.088 ± 0.010 | 1.4 ± 0.2 | 0.0076 |

**Km (nM) derived from Michaelis-Menten Fit* ***Not applicable*

**Supplementary Table S4. Tabulated cBioPortal mutations to ASXL1.**
Table showing mutations from cBioPoral (*67, 68*) to ASXL1 that interface with DNA dyad, DNA exit, and ubiquitin patch. Columns show study of origin, cancer type, and protein change.

| Study of Origin | Cancer Type Detailed | Protein Change |
|---|---|---|
| Upper Tract Urothelial Carcinoma (MSK, Nat Commun 2020)(*69*) | Upper Tract Urothelial Carcinoma | **R244C** |
| Upper Tract Urothelial Cancer (MSK, Eur Urol 2015)(*70*) | Upper Tract Urothelial Carcinoma | **R244C** |
| Glioma (MSK, Nature 2019)(*69*) | Glioblastoma Multiforme | **R244H** |
| Uterine Corpus Endometrial Carcinoma (TCGA, PanCancer Atlas)(*71*) | Uterine Endometrioid Carcinoma | **R244H** |
| Uterine Corpus Endometrial Carcinoma (TCGA, PanCancer Atlas)(*71*) | Uterine Endometrioid Carcinoma | **R244H** |
| Myelodysplastic Syndromes (MDS IWG, IPSSM, NEJM Evidence 2022)(*72*) | Myelodysplastic Syndromes | **R244H** |
| Uterine Corpus Endometrial Carcinoma (TCGA, PanCancer Atlas)(*71*) | Uterine Endometrioid Carcinoma | **R246I** |
| MSK-IMPACT Clinical Sequencing Cohort (MSKCC, Nat Med 2017)(*73*) | High-Grade Serous Ovarian Cancer | **R265C** |
| Endometrial Carcinoma MSI (MSK, Clin Cancer Res 2022)(*74*) | Endometrial Carcinoma | **R265C** |
| Colorectal Adenocarcinoma (TCGA, PanCancer Atlas)(*71*) | Colon Adenocarcinoma | **R265H** |
| China Pan-cancer (OrigiMed, Nature 2022)(*75*) | Uterine Endometrioid Carcinoma | **R265S** |
| Uterine Corpus Endometrial Carcinoma (TCGA, PanCancer Atlas)(*71*) | Uterine Endometrioid Carcinoma | **R265S** |
| China Pan-cancer (OrigiMed, Nature 2022)(*75*) | Lung Adenocarcinoma | **N309S** |
| Diffuse Glioma (GLASS Consortium, Nature 2019)(*76*) | Glioblastoma | **T314I** |
| Uterine Corpus Endometrial Carcinoma (TCGA, PanCancer Atlas)(*71*) | Uterine Endometrioid Carcinoma | **T314Yfs*13** |
| Lung Squamous Cell Carcinoma (TCGA, PanCancer Atlas)(*71*) | Lung Squamous Cell Carcinoma | **H315N** |
| MSK-IMPACT Clinical Sequencing Cohort (MSKCC, Nat Med 2017)(*73*) | Colon Adenocarcinoma | **H315R** |
| MSK-IMPACT Clinical Sequencing Cohort (MSKCC, Nat Med 2017)(*73*) | Cutaneous Melanoma | **H315Y** |
| Cholangiocarcinoma (ICGC, Cancer Discov 2017)(*77*) | Cholangiocarcinoma | **R338Q** |
| China Pan-cancer (OrigiMed, Nature 2022)(*75*) | Colorectal Adenocarcinoma | **R338Q** |
| China Pan-cancer (OrigiMed, Nature 2022)(*75*) | Colorectal Adenocarcinoma | **K345N** |

**Supplementary Table S5. Tabulated cBioPortal mutations to BAP1.**
Table showing mutations from cBioPoral (*67, 68*) to BAP1 that interface with acidic patch, DNA dyad, DNA exit, and ubiquitin patch. Columns show study of origin, cancer type, and protein change.

| Study of Origin | Cancer Type Detailed | Protein Change |
|---|---|---|
| Adenoid Cystic Carcinoma Project (J Clin Invest 2019)(*78*) | Adenoid Cystic Carcinoma | **D11Afs*58** |
| China Pan-cancer (OrigiMed, Nature 2022)(*75*) | Intrahepatic Cholangiocarcinoma | **D11N** |
| China Pan-cancer (OrigiMed, Nature 2022)(*75*) | Gastric Adenocarcinoma | **D11N** |
| Cholangiocarcinoma (ICGC, Cancer Discov 2017)(*77*) | Cholangiocarcinoma | **E31del** |
| Ovarian Serous Cystadenocarcinoma (TCGA, PanCancer Atlas)(*71*) | Serous Ovarian Cancer | **E31del** |
| MSK-IMPACT Clinical Sequencing Cohort (MSKCC, Nat Med 2017)(*73*) | Cutaneous Melanoma | **E31del** |
| MSK-IMPACT Clinical Sequencing Cohort (MSKCC, Nat Med 2017)(*73*) | Unclassified Renal Cell Carcinoma | **E31del** |
| China Pan-cancer (OrigiMed, Nature 2022)(*75*) | Liver Hepatocellular Carcinoma | **E31del** |
| Adenoid Cystic Carcinoma Project (J Clin Invest 2019)(*78*) | Adenoid Cystic Carcinoma | **E31*** |
| Kidney Renal Clear Cell Carcinoma (TCGA, PanCancer Atlas)(*71*) | Renal Clear Cell Carcinoma | **E31A** |
| Uterine Corpus Endometrial Carcinoma (TCGA, PanCancer Atlas)(*71*) | Uterine Endometrioid Carcinoma | **E31D** |
| Hepatocellular Carcinomas (INSERM, Nat Genet 2015)(*79*) | Hepatocellular Carcinoma | **E31Gfs*41** |
| Kidney Renal Papillary Cell Carcinoma (TCGA, PanCancer Atlas)(*71*) | Papillary Renal Cell Carcinoma | **E31G** |
| China Pan-cancer (OrigiMed, Nature 2022)(*75*) | Renal Clear Cell Carcinoma | **E31G** |
| Bladder Cancer (MSKCC, Eur Urol 2014)(*80*) | Bladder Urothelial Carcinoma | **E31K** |
| China Pan-cancer (OrigiMed, Nature 2022)(*75*) | Perihilar Cholangiocarcinoma | **E31K** |
| Urothelial Carcinoma (BCAN/HCRN 2022)(*81*) | Bladder Urothelial Carcinoma | **E31Q** |
| Renal Clear Cell Carcinoma (UTokyo, Nat Genet 2013)(*82*) | Renal Clear Cell Carcinoma with Sarcomatoid Features | **E31V** |
| China Pan-cancer (OrigiMed, Nature 2022)(*75*) | Renal Clear Cell Carcinoma | **E31V** |
| MSK-IMPACT Clinical Sequencing Cohort (MSKCC, Nat Med 2017)(*73*) | Oligodendroglioma | **Y33del** |
| Uveal Melanoma (TCGA, PanCancer Atlas)(*71*) | Uveal Melanoma | **Y33*** |
| Combined Hepatocellular and Intrahepatic Cholangiocarcinoma (Peking University, Cancer Cell 2019)(*83*) | Hepatocellular Carcinoma plus Intrahepatic Cholangiocarcinoma | **Y33*** |
| Combined Hepatocellular and Intrahepatic Cholangiocarcinoma (Peking University, Cancer Cell 2019)(*83*) | Hepatocellular Carcinoma plus Intrahepatic Cholangiocarcinoma | **Y33*** |
| Breast Cancer (METABRIC, Nature 2012 & Nat Commun 2016)(*84, 85*) | Breast Invasive Ductal Carcinoma | **Y33*** |
| Stomach Adenocarcinoma (TCGA, PanCancer Atlas)(*71*) | Diffuse Type Stomach Adenocarcinoma | **Y33*** |
| Kidney Renal Papillary Cell Carcinoma (TCGA, PanCancer Atlas)(*71*) | Papillary Renal Cell Carcinoma | **Y33C** |
| China Pan-cancer (OrigiMed, Nature 2022)(*75*) | Intrahepatic Cholangiocarcinoma | **Y33Rfs*36** |
| Cutaneous Squamous Cell Carcinoma (DFCI, Clin Cancer Res 2015)(*86*) | Cutaneous Squamous Cell Carcinoma | **L35F** |
| Skin Cutaneous Melanoma (TCGA, PanCancer Atlas)(*71*) | Cutaneous Melanoma | **L35R** |
| Stomach Adenocarcinoma (U Tokyo, Nat Genet 2014)(*87*) | Stomach Adenocarcinoma | **R56C** |
| MSK-IMPACT Clinical Sequencing Cohort (MSKCC, Nat Med 2017)(*73*) | Bladder Urothelial Carcinoma | **R56C** |
| Breast Cancer (METABRIC, Nature 2012 & Nat Commun 2016)(*84, 85*) | Breast Invasive Ductal Carcinoma | **R56C** |
| Breast Cancer (METABRIC, Nature 2012 & Nat Commun 2016)(*84, 85*) | Breast Invasive Ductal Carcinoma | **R56C** |
| Uterine Corpus Endometrial Carcinoma (TCGA, PanCancer Atlas)(*71*) | Uterine Endometrioid Carcinoma | **R56C** |
| China Pan-cancer (OrigiMed, Nature 2022)(*75*) | Esophageal Squamous Cell Carcinoma | **R56H** |

| | | |
|---|---|---|
| Upper Tract Urothelial Carcinoma (MSK, Nat Commun 2020)(*69*) | Upper Tract Urothelial Carcinoma | **R57Q** |
| MSK-IMPACT Clinical Sequencing Cohort (MSKCC, Nat Med 2017)(*73*) | Upper Tract Urothelial Carcinoma | **R57Q** |
| Pediatric Brain Cancer (CPTAC/CHOP, Cell 2020)(*88*) | Medulloblastoma | **R57W** |
| Pediatric Brain Cancer (CPTAC/CHOP, Cell 2020)(*88*) | Medulloblastoma | **R57W** |
| Skin Cutaneous Melanoma (Yale, Nat Genet 2012)(*89*) | Cutaneous Melanoma | **R57_R60del** |
| MSK-IMPACT Clinical Sequencing Cohort (MSKCC, Nat Med 2017)(*73*) | Upper Tract Urothelial Carcinoma | **R59Q** |
| MSK-IMPACT Clinical Sequencing Cohort (MSKCC, Nat Med 2017)(*73*) | Colorectal Adenocarcinoma | **R59Q** |
| China Pan-cancer (OrigiMed, Nature 2022)(*75*) | Gastric Adenocarcinoma | **R59Q** |
| Prostate Adenocarcinoma (SMMU, Eur Urol 2017)(*90*) | Prostate Adenocarcinoma | **R59Q** |
| Skin Cutaneous Melanoma (TCGA, PanCancer Atlas)(*71*) | Cutaneous Melanoma | **R59W** |
| Cholangiocarcinoma (ICGC, Cancer Discov 2017)(*77*) | Cholangiocarcinoma | **R59W** |
| MSK-IMPACT Clinical Sequencing Cohort (MSKCC, Nat Med 2017)(*73*) | Uveal Melanoma | **R60*** |
| China Pan-cancer (OrigiMed, Nature 2022)(*75*) | Pancreatic Adenocarcinoma | **R60*** |
| Endometrial Carcinoma MSI (MSK, Clin Cancer Res 2022)(*74*) | Endometrial Carcinoma | **R60Q** |
| MSK-IMPACT Clinical Sequencing Cohort (MSKCC, Nat Med 2017)(*73*) | Intrahepatic Cholangiocarcinoma | **C91F** |
| MSK-IMPACT Clinical Sequencing Cohort (MSKCC, Nat Med 2017)(*73*) | Renal Clear Cell Carcinoma | **C91F** |
| China Pan-cancer (OrigiMed, Nature 2022)(*75*) | Renal Clear Cell Carcinoma | **C91F** |
| Mesothelioma (TCGA, PanCancer Atlas)(*71*) | Pleural Mesothelioma, Epithelioid Type | **C91G** |
| Renal Clear Cell Carcinoma (UTokyo, Nat Genet 2013)(*82*) | Renal Clear Cell Carcinoma with Sarcomatoid Features | **C91G** |
| MSK-IMPACT Clinical Sequencing Cohort (MSKCC, Nat Med 2017)(*73*) | Bladder Urothelial Carcinoma | **C91R** |
| China Pan-cancer (OrigiMed, Nature 2022)(*75*) | Intrahepatic Cholangiocarcinoma | **C91R** |
| Urothelial Carcinoma (BCAN/HCRN 2022)(*81*) | Bladder Urothelial Carcinoma | **C91R** |
| Pan-cancer Analysis of Advanced and Metastatic Tumors (BCGSC, Nature Cancer 2020)(*91*) | Basal Cell Carcinoma | **C91S** |
| China Pan-cancer (OrigiMed, Nature 2022)(*75*) | Perihilar Cholangiocarcinoma | **C91W** |
| Pleural Mesothelioma (NYU, Cancer Res 2015)(*92*) | Pleural Mesothelioma | **C91Y** |
| Urothelial Carcinoma (BCAN/HCRN 2022)(*81*) | Bladder Urothelial Carcinoma | **C91Y** |
| MSK-IMPACT Clinical Sequencing Cohort (MSKCC, Nat Med 2017)(*73*) | Cholangiocarcinoma | **R146K** |
| SUMMIT - Neratinib Basket Study (Multi-Institute, Nature 2018)(*93*) | Cholangiocarcinoma | **R146K** |
| Metastatic Biliary Tract Cancers (SUMMIT - Neratinib Basket Trial, 2022) | Cholangiocarcinoma | **R146K** |
| China Pan-cancer (OrigiMed, Nature 2022)(*75*) | Intrahepatic Cholangiocarcinoma | **R146M** |
| Diffuse Glioma (GLASS Consortium, Nature 2019)(*76*) | Glioblastoma | **X146_splice** |
| Cholangiocarcinoma (ICGC, Cancer Discov 2017)(*77*) | Cholangiocarcinoma | **X146_splice** |
| Cholangiocarcinoma (ICGC, Cancer Discov 2017)(*77*) | Cholangiocarcinoma | **X146_splice** |
| Pan-cancer Analysis of Advanced and Metastatic Tumors (BCGSC, Nature Cancer 2020)(*91*) | Pancreatic Adenocarcinoma | **X146_splice** |
| MSK-IMPACT Clinical Sequencing Cohort (MSKCC, Nat Med 2017)(*73*) | Intrahepatic Cholangiocarcinoma | **X146_splice** |
| MSK-IMPACT Clinical Sequencing Cohort (MSKCC, Nat Med 2017)(*73*) | Pleural Mesothelioma | **X146_splice** |
| MSK-IMPACT Clinical Sequencing Cohort (MSKCC, Nat Med 2017)(*73*) | Uveal Melanoma | **X146_splice** |
| Pan-cancer analysis of whole genomes (ICGC/TCGA, Nature 2020)(*94*) | Hepatocellular Carcinoma | **X146_splice** |

| | | |
|---|---|---|
| China Pan-cancer (OrigiMed, Nature 2022)(*75*) | Colorectal Adenocarcinoma | **X146_splice** |
| China Pan-cancer (OrigiMed, Nature 2022)(*75*) | Gastric Adenocarcinoma | **X146_splice** |
| China Pan-cancer (OrigiMed, Nature 2022)(*75*) | Colorectal Adenocarcinoma | **X146_splice** |
| Liver Hepatocellular Carcinoma (TCGA, PanCancer Atlas)(*71*) | Hepatocellular Carcinoma | **X146_splice** |
| Clear Cell Renal Cell Carcinoma (DFCI, Science 2019)(*95*) | Renal Clear Cell Carcinoma | **R227Afs*4** |
| MSK-IMPACT Clinical Sequencing Cohort (MSKCC, Nat Med 2017)(*73*) | Prostate Adenocarcinoma | **R227C** |
| MSK-IMPACT Clinical Sequencing Cohort (MSKCC, Nat Med 2017)(*73*) | Prostate Adenocarcinoma | **R227C** |
| Adenoid Cystic Carcinoma Project (J Clin Invest 2019)(*78*) | Adenoid Cystic Carcinoma | **R227Hfs*18** |
| China Pan-cancer (OrigiMed, Nature 2022)(*75*) | Gastric Adenocarcinoma | **R227Hfs*17** |
| Pan-cancer analysis of whole genomes (ICGC/TCGA, Nature 2020)(*94*) | Lung Squamous Cell Carcinoma | **R227H** |
| China Pan-cancer (OrigiMed, Nature 2022)(*75*) | Perihilar Cholangiocarcinoma | **R227H** |
| Upper Tract Urothelial Carcinoma (MSK, Nat Commun 2020)(*69*) | Upper Tract Urothelial Carcinoma | **R227L** |
| Upper Tract Urothelial Cancer (MSK, Eur Urol 2015)(*70*) | Upper Tract Urothelial Carcinoma | **R227L** |
| Upper Tract Urothelial Carcinoma (MSK, Nat Commun 2020)(*69*) | Upper Tract Urothelial Carcinoma | **R227P** |
| Upper Tract Urothelial Cancer (MSK, Eur Urol 2015)(*70*) | Upper Tract Urothelial Carcinoma | **R227P** |
| Adenoid Cystic Carcinoma Project (J Clin Invest 2019)(*78*) | Adenoid Cystic Carcinoma | **R227P** |
| Adenoid Cystic Carcinoma Project (J Clin Invest 2019)(*78*) | Adenoid Cystic Carcinoma | **R227P** |
| MSK-IMPACT Clinical Sequencing Cohort (MSKCC, Nat Med 2017)(*73*) | Upper Tract Urothelial Carcinoma | **R227P** |
| MSK-IMPACT Clinical Sequencing Cohort (MSKCC, Nat Med 2017)(*73*) | Bladder Urothelial Carcinoma | **R227P** |
| China Pan-cancer (OrigiMed, Nature 2022)(*75*) | Thymic Carcinoma | **R227P** |
| China Pan-cancer (OrigiMed, Nature 2022)(*75*) | Pancreatic Adenocarcinoma | **R227P** |
| Urothelial Carcinoma (BCAN/HCRN 2022)(*81*) | Bladder Urothelial Carcinoma | **R227P** |
| China Pan-cancer (OrigiMed, Nature 2022)(*75*) | Head and Neck Squamous Cell Carcinoma | **L230P** |
| Renal Clear Cell Carcinoma (UTokyo, Nat Genet 2013)(*82*) | Renal Clear Cell Carcinoma with Sarcomatoid Features | **L230Q** |
| Uterine Corpus Endometrial Carcinoma (TCGA, PanCancer Atlas)(*71*) | Uterine Endometrioid Carcinoma | **D672N** |
| Breast Cancer (METABRIC, Nature 2012 & Nat Commun 2016)(*84, 85*) | Breast Invasive Ductal Carcinoma | **R699P** |
| Uveal Melanoma (QIMR, Oncotarget 2016)(*96*) | Uveal Melanoma | **R699Qfs*6** |
| China Pan-cancer (OrigiMed, Nature 2022)(*75*) | Pancreatic Neuroendocrine Tumor | **R699Q** |
| MSK-IMPACT Clinical Sequencing Cohort (MSKCC, Nat Med 2017)(*73*) | Colorectal Adenocarcinoma | **R699W** |
| Breast Cancer (METABRIC, Nature 2012 & Nat Commun 2016)(*84, 85*) | Breast Invasive Ductal Carcinoma | **R699W** |
| China Pan-cancer (OrigiMed, Nature 2022)(*75*) | Lung Squamous Cell Carcinoma | **R700L** |
| Pan-cancer analysis of whole genomes (ICGC/TCGA, Nature 2020)(*94*) | Head and Neck Squamous Cell Carcinoma | **R700Q** |
| China Pan-cancer (OrigiMed, Nature 2022)(*75*) | Small Bowel Adenocarcinoma | **R700Q** |
| Uterine Corpus Endometrial Carcinoma (TCGA, PanCancer Atlas)(*71*) | Uterine Endometrioid Carcinoma | **R700Q** |
| Stomach Adenocarcinoma (TCGA, PanCancer Atlas)(*71*) | Stomach Adenocarcinoma | **R700Q** |
| Colon Cancer (CPTAC-2 Prospective, Cell 2019)(*97*) | Colon Adenocarcinoma | **R700W** |
| China Pan-cancer (OrigiMed, Nature 2022)(*75*) | Colorectal Adenocarcinoma | **R700W** |
| Uterine Corpus Endometrial Carcinoma (TCGA, PanCancer Atlas)(*71*) | Uterine Endometrioid Carcinoma | **R700W** |

| | | |
|---|---|---|
| Uterine Corpus Endometrial Carcinoma (TCGA, PanCancer Atlas)(*71*) | Uterine Endometrioid Carcinoma | **R700W** |
| Non-Small Cell Lung Cancer (TRACERx, NEJM & Nature 2017)(*98*) | Non-Small Cell Lung Cancer | **R701C** |
| Non-Small Cell Lung Cancer (TRACERx, NEJM & Nature 2017)(*98*) | Non-Small Cell Lung Cancer | **R701C** |
| Non-Small Cell Lung Cancer (TRACERx, NEJM & Nature 2017)(*98*) | Non-Small Cell Lung Cancer | **R701C** |
| MSK-IMPACT Clinical Sequencing Cohort (MSKCC, Nat Med 2017)(*73*) | Adrenocortical Carcinoma | **R701C** |

## REFERENCES AND NOTES


1. A. P. Szczepanski, L. Wang, Emerging multifaceted roles of BAP1 complexes in biological processes. *Cell Death Discov.* **7**, 20 (2021).

2. J. C. Scheuermann, A. G. de Ayala Alonso, K. Oktaba, N. Ly-Hartig, R. K. McGinty, S. Fraterman, M. Wilm, T. W. Muir, J. Müller, Histone H2A deubiquitinase activity of the Polycomb repressive complex PR-DUB. *Nature* **465**, 243–247 (2010).

3. D. D. Sahtoe, W. J. Van Dijk, R. Ekkebus, H. Ovaa, T. K. Sixma, BAP1/ASXL1 recruitment and activation for H2A deubiquitination. *Nat. Commun.* **7**, 10292 (2016).

4. L. Sanchez-Pulido, L. Kong, C. P. Ponting, A common ancestry for BAP1 and Uch37 regulators. *Bioinformatics* **28**, 1953–1956 (2012).

5. N. A. Fursova, A. H. Turberfield, N. P. Blackledge, E. L. Findlater, A. Lastuvkova, M. K. Huseyin, P. Dobrinić, R. J. Klose, BAP1 constrains pervasive H2AK119ub1 to control the transcriptional potential of the genome. *Genes Dev.* **35**, 749–770 (2021).

6. E. Conway, F. Rossi, D. Fernandez-Perez, E. Ponzo, K. J. Ferrari, M. Zanotti, D. Manganaro, S. Rodighiero, S. Tamburri, D. Pasini, BAP1 enhances Polycomb repression by counteracting widespread H2AK119ub1 deposition and chromatin condensation. *Mol. Cell* **81**, 3526–3541.e8 (2021).

7. J. N. Kuznetsov, T. H. Aguero, D. A. Owens, S. Kurtenbach, M. G. Field, M. A. Durante, D. A. Rodriguez, M. L. King, J. W. Harbour, BAP1 regulates epigenetic switch from pluripotency to differentiation in developmental lineages giving rise to BAP1-mutant cancers. *Sci. Adv.* **5**, eaax1738 (2019).

8. A. Campagne, M. K. Lee, D. Zielinski, A. Michaud, S. le Corre, F. Dingli, H. Chen, L. Z. Shahidian, I. Vassilev, N. Servant, D. Loew, E. Pasmant, S. Postel-Vinay, M. Wassef, R. Margueron, BAP1 complex promotes transcription by opposing PRC1-mediated H2A ubiquitylation. *Nat. Commun.* **10**, 348 (2019).

9. J. Bonnet, I. Boichenko, R. Kalb, M. le Jeune, S. Maltseva, M. Pieropan, K. Finkl, B. Fierz, J. Müller, PR-DUB preserves Polycomb repression by preventing excessive accumulation of H2Aub1, an antagonist of chromatin compaction. *Genes Dev.* **36**, 1046–1061 (2022).

10. Y. B. Schwartz, V. Pirrotta, Polycomb silencing mechanisms and the management of genomic programmes. *Nat. Rev. Genet.* **8**, 9–22 (2007).

11. L.-H. Wang, M. A. E. Aberin, S. Wu, S.-P. Wang, The MLL3/4 H3K4 methyltransferase complex in establishing an active enhancer landscape. *Biochem. Soc. Trans.* **49**, 1041–1054 (2021).

12. L. Wang, Z. Zhao, P. A. Ozark, D. Fantini, S. A. Marshall, E. J. Rendleman, K. A. Cozzolino, N. Louis, X. He, M. A. Morgan, Y. H. Takahashi, C. K. Collings, E. R. Smith, P. Ntziachristos, J. N. Savas, L. Zou, R. Hashizume, J. J. Meeks, A. Shilatifard, Resetting the epigenetic balance of Polycomb and COMPASS function at enhancers for cancer therapy. *Nat. Med.* **24**, 758–769 (2018).

13. I. H. Ismail, R. Davidson, J. P. Gagné, Z. Z. Xu, G. G. Poirier, M. J. Hendzel, Germline mutations in BAP1 impair its function in DNA double-strand break repair. *Cancer Res.* **74**, 4282–4294 (2014).

14. O. Abdel-Wahab, J. Gao, M. Adli, A. Dey, T. Trimarchi, Y. R. Chung, C. Kuscu, T. Hricik, D. Ndiaye-Lobry, L. M. LaFave, R. Koche, A. H. Shih, O. A. Guryanova, E. Kim, S. Li, S. Pandey, J. Y. Shin, L. Telis, J. Liu, P. K. Bhatt, S. Monette, X. Zhao, C. E. Mason, C. Y. Park, B. E. Bernstein, I. Aifantis, R. L. Levine, Deletion of Asxl1 results in myelodysplasia and severe developmental defects in vivo. *J. Exp. Med.* **210**, 2641–2659 (2013).

15. M. Cigognetti, S. Lonardi, S. Fisogni, P. Balzarini, V. Pellegrini, A. Tironi, L. Bercich, M. Bugatti, G. Rossi, B. Murer, M. Barbareschi, S. Giuliani, A. Cavazza, G. Marchetti, W. Vermi, F. Facchetti, BAP1 (BRCA1-associated protein 1) is a highly specific marker for differentiating mesothelioma from reactive mesothelial proliferations. *Mod. Pathol.* **28**, 1043–1057 (2015).

16. M. Cheung, J. R. Testa, BAP1, a tumor suppressor gene driving malignant mesothelioma. *Transl. Lung Cancer Res.* **6**, 270–278 (2017).

17. F. Matheus, E. Rusha, R. Rehimi, L. Molitor, A. Pertek, M. Modic, R. Feederle, A. Flatley, E. Kremmer, A. Geerlof, V. Rishko, A. Rada-Iglesias, M. Drukker, Pathological ASXL1 mutations and protein variants impair neural crest development. *Stem Cell Rep.* **12**, 861–868 (2019).

18. L. Shahriyari, M. Abdel-Rahman, C. Cebulla, BAP1 expression is prognostic in breast and uveal melanoma but not colon cancer and is highly positively correlated with RBM15B and USP19. *PLOS ONE* **14**, e0211507 (2019).

19. G. Stålhammar, T. R. O. See, S. Phillips, S. Seregard, H. E. Grossniklaus, Digital image analysis of BAP-1 accurately predicts uveal melanoma metastasis. *Transl. Vis. Sci. Technol.* **8**, 11 (2019).

20. I. De, E. C. Chittock, H. Grötsch, T. C. R. Miller, A. A. McCarthy, C. W. Müller, Structural basis for the activation of the deubiquitinase calypso by the polycomb protein ASX. *Structure* **27**, 528–536.e4 (2019).

21. M. Foglizzo, A. J. Middleton, A. E. Burgess, J. M. Crowther, R. C. J. Dobson, J. M. Murphy, C. L. Day, P. D. Mace, A bidentate Polycomb repressive-deubiquitinase complex is required for efficient activity on nucleosomes. *Nat. Commun.* **9**, 3932 (2018).

22. D. D. Sahtoe, W. J. van Dijk, F. E. Oualid, R. Ekkebus, H. Ovaa, T. K. Sixma, Mechanism of UCH-L5 activation and inhibition by DEUBAD domains in RPN13 and INO80G. *Mol. Cell* **57**, 887–900 (2015).

23. L. Long, M. Furgason, T. Yao, Generation of nonhydrolyzable ubiquitin-histone mimics. *Methods* **70**, 134–138 (2014).

24. H. Stark, GraFix: Stabilization of fragile macromolecular complexes for single particle cryo-EM. *Methods Enzymol.* **481**, 109–126 (2010).

25. R. Evans, M. O'Neill, A. Pritzel, N. Antropova, A. Senior, T. Green, A. Žídek, R. Bates, S. Blackwell, J. Yim, O. Ronneberger, S. Bodenstein, M. Zielinski, A. Bridgland, A. Potapenko, A. Cowie, K. Tunyasuvunakool, R. Jain, E. Clancy, P. Kohli, J. Jumper, D. Hassabis, Protein complex prediction with AlphaFold-multimer. bioRxiv 2021.10.04.463034 (2022). https://doi.org/10.1101/2021.10.04.463034.

26. D. Komander, M. Rape, The ubiquitin code. *Annu. Rev. Biochem.* **81**, 203–229 (2012).

27. M. I. Valencia-Sánchez, P. de Ioannes, M. Wang, D. M. Truong, R. Lee, J. P. Armache, J. D. Boeke, K. J. Armache, Regulation of the Dot1 histone H3K79 methyltransferase by histone H4K16 acetylation. *Science* **371**, eabc6663 (2021).

28. E. J. Worden, X. Zhang, C. Wolberger, Structural basis for COMPASS recognition of an H2B-ubiquitinated nucleosome. *eLife* **9**, e53199 (2020).

29. H. Peng, J. Prokop, J. Karar, K. Park, L. Cao, J. W. Harbour, A. M. Bowcock, S. B. Malkowicz, M. Cheung, J. R. Testa, F. J. Rauscher III, Familial and somatic BAP1 mutations inactivate ASXL1/2-mediated allosteric regulation of BAP1 deubiquitinase by targeting multiple independent domains. *Cancer Res.* **78**, 1200–1213 (2018).

30. C. A. Davey, D. F. Sargent, K. Luger, A. W. Maeder, T. J. Richmond, Solvent mediated interactions in the structure of the nucleosome core particle at 1.9 a resolution. *J. Mol. Biol.* **319**, 1097–1113 (2002).

31. V. Kasinath, C. Beck, P. Sauer, S. Poepsel, J. Kosmatka, M. Faini, D. Toso, R. Aebersold, E. Nogales, JARID2 and AEBP2 regulate PRC2 in the presence of H2AK119ub1 and other histone modifications. *Science* **371**, eabc3393 (2021).

32. M. I. Valencia-Sánchez, P. De Ioannes, M. Wang, N. Vasilyev, R. Chen, E. Nudler, J.-P. Armache, K.-J. Armache, Structural basis of Dot1L stimulation by histone H2B lysine 120 ubiquitination. *Mol. Cell* **74**, 1010–1019.e6 (2019).

33. R. K. McGinty, S. Tan, Recognition of the nucleosome by chromatin factors and enzymes. *Curr. Opin. Struct. Biol.* **37**, 54–61 (2016).

34. R. K. Mcginty, R. C. Henrici, S. Tan, Crystal structure of the PRC1 ubiquitylation module bound to the nucleosome. *Nature* **514**, 591–596 (2014).

35. R. D. Makde, J. R. England, H. P. Yennawar, S. Tan, Structure of RCC1 chromatin factor bound to the nucleosome core particle. *Nature* **467**, 562–566 (2010).

36. A. J. Barbera, J. V. Chodaparambil, B. Kelley-Clarke, V. Joukov, J. C. Walter, K. Luger, K. M. Kaye, The nucleosomal surface as a docking station for Kaposi's sarcoma herpesvirus LANA. *Science* **311**, 856–861 (2006).

37. K. J. Armache, J. D. Garlick, D. Canzio, G. J. Narlikar, R. E. Kingston, Structural basis of silencing: Sir3 BAH domain in complex with a nucleosome at 3.0 Å resolution. *Science* **334**, 977–982 (2011).

38. E. J. Worden, N. A. Hoffmann, C. W. Hicks, C. Wolberger, Mechanism of cross-talk between H2B ubiquitination and H3 methylation by Dot1L. *Cell* **176**, 1490–1501.e12 (2019).

39. M. Carbone, J. W. Harbour, J. Brugarolas, A. Bononi, I. Pagano, A. Dey, T. Krausz, H. I. Pass, H. Yang, G. Gaudino, Biological mechanisms and clinical significance of BAP1 mutations in human cancer. *Cancer Discov.* **10**, 1103–1120 (2020).

40. H. Yang, S. Kurtenbach, Y. Guo, I. Lohse, M. A. Durante, J. Li, Z. Li, H. al-Ali, L. Li, Z. Chen, M. G. Field, P. Zhang, S. Chen, S. Yamamoto, Z. Li, Y. Zhou, S. D. Nimer, J. W. Harbour, C. Wahlestedt, M. Xu, F. C. Yang, Gain of function of ASXL1 truncating protein in the pathogenesis of myeloid malignancies. *Blood* **131**, 328–341 (2018).

41. L. Wang, N. W. Birch, Z. Zhao, C. M. Nestler, A. Kazmer, A. Shilati, A. Blake, P. A. Ozark, E. J. Rendleman, D. Zha, C. A. Ryan, M. A. J. Morgan, A. Shilatifard, Epigenetic targeted therapy of stabilized BAP1 in ASXL1 gain-of-function mutated leukemia. *Nat. Cancer* **2**, 515–526 (2021).

42. A. Skrajna, D. Goldfarb, K. M. Kedziora, E. M. Cousins, G. D. Grant, C. J. Spangler, E. H. Barbour, X. Yan, N. A. Hathaway, N. G. Brown, J. G. Cook, M. B. Major, R. K. McGinty, Comprehensive nucleosome interactome screen establishes fundamental principles of nucleosome binding. *Nucleic Acids Res.* **48**, 9415–9432 (2020).

43. D. Grau, Y. Zhang, C. H. Lee, M. Valencia-Sánchez, J. Zhang, M. Wang, M. Holder, V. Svetlov, D. Tan, E. Nudler, D. Reinberg, T. Walz, K. J. Armache, Structures of monomeric and dimeric PRC2:EZH1 reveal flexible modules involved in chromatin compaction. *Nat. Commun.* **12**, 714 (2021).

44. M. Dombrowski, M. Engeholm, C. Dienemann, S. Dodonova, P. Cramer, Histone H1 binding to nucleosome arrays depends on linker DNA length and trajectory. *Nat. Struct. Mol. Biol.* **29**, 493–501 (2022).

45. B.-R. Zhou, H. Feng, S. Kale, T. Fox, H. Khant, N. de Val, R. Ghirlando, A. R. Panchenko, Y. Bai, Distinct structures and dynamics of chromatosomes with different human linker histone isoforms. *Mol. Cell* **81**, 166–182.e6 (2021).

46. W. Ge, C. Yu, J. Li, Z. Yu, X. Li, Y. Zhang, C. P. Liu, Y. Li, C. Tian, X. Zhang, G. Li, B. Zhu, R. M. Xu, Basis of the H2AK119 specificity of the Polycomb repressive deubiquitinase. *Nature* **616**, 176–182 (2023).

47. R. Meas, P. Mao, Histone ubiquitylation and its roles in transcription and DNA damage response. *DNA Repair* **36**, 36–42 (2015).

48. P. N. Dyer, R. S. Edayathumangalam, C. L. White, Y. Bao, S. Chakravarthy, U. M. Muthurajan, K. Luger, Reconstitution of nucleosome core particles from recombinant histones and DNA. *Methods Enzymol.* **375**, 23–44 (2004).

49. H. T. Dao, H. Liu, N. Mashtalir, C. Kadoch, T. W. Muir, Synthesis of oriented hexasomes and asymmetric nucleosomes using a template editing process. *J. Am. Chem. Soc.* **144**, 2284–2291 (2022).

50. L. F. Schachner, K. Jooß, M. A. Morgan, A. Piunti, M. J. Meiners, J. O. Kafader, A. S. Lee, M. Iwanaszko, M. A. Cheek, J. M. Burg, S. A. Howard, M. C. Keogh, A. Shilatifard, N. L. Kelleher, Decoding the protein composition of whole nucleosomes with Nuc-MS. *Nat. Methods* **18**, 303–308 (2021).

51. M. R. Marunde, H. A. Fuchs, J. M. Burg, I. K. Popova, A. Vaidya, N. W. Hall, M. J. Meiners, R. Watson, S. A. Howard, K. Novitzky, E. M. Anarney, M. A. Cheek, Z.-W. Sun, B. J. Venters, M.-C. Keogh, C. A. Musselman, Nucleosome conformation dictates the histone code. bioRxiv 2022.02.21.481373 (2022). https://doi.org/10.1101/2022.02.21.481373.

52. X. Bi, R. Yang, X. Feng, D. Rhodes, C. F. Liu, Semisynthetic UbH2A reveals different activities of deubiquitinases and inhibitory effects of H2A K119 ubiquitination on H3K36 methylation in mononucleosomes. *Org. Biomol. Chem.* **14**, 835–839 (2016).

53. Y. S. Choi, S. A. Bollinger, L. F. Prada, F. Scavone, T. Yao, R. E. Cohen, High-affinity free ubiquitin sensors for quantifying ubiquitin homeostasis and deubiquitination. *Nat. Methods* **16**, 771–777 (2019).

54. X. Li, P. Mooney, S. Zheng, C. R. Booth, M. B. Braunfeld, S. Gubbens, D. A. Agard, Y. Cheng, Electron counting and beam-induced motion correction enable near-atomic-resolution single-particle cryo-EM. *Nat. Methods* **10**, 584–590 (2013).

55. A. Cheng, C. Negro, J. F. Bruhn, W. J. Rice, S. Dallakyan, E. T. Eng, D. G. Waterman, C. S. Potter, B. Carragher, Leginon: New features and applications. *Protein Sci.* **30**, 136–150 (2021).

56. S. Q. Zheng, E. Palovcak, J. P. Armache, K. A. Verba, Y. Cheng, D. A. Agard, MotionCor2: Anisotropic correction of beam-induced motion for improved cryo-electron microscopy. *Nat. Methods* **14**, 331–332 (2017).

57. J. Zivanov, T. Nakane, B. O. Forsberg, D. Kimanius, W. J. H. Hagen, E. Lindahl, S. H. W. Scheres, New tools for automated high-resolution cryo-EM structure determination in RELION-3. *eLife* **7**, e42166 (2018).

58. A. Punjani, J. L. Rubinstein, D. J. Fleet, M. A. Brubaker, cryoSPARC: Algorithms for rapid unsupervised cryo-EM structure determination. *Nat. Methods* **14**, 290–296 (2017).

59. J. Zivanov, T. Nakane, S. H. W. Scheres, A Bayesian approach to beam-induced motion correction in cryo-EM single-particle analysis. *IUCrJ* **6**, 5–17 (2019).

60. K. Zhang, Gctf: Real-time CTF determination and correction. *J. Struct. Biol.* **193**, 1–12 (2016).

61. E. F. Pettersen, T. D. Goddard, C. C. Huang, G. S. Couch, D. M. Greenblatt, E. C. Meng, T. E. Ferrin, UCSF Chimera—A visualization system for exploratory research and analysis. *J. Comput. Chem.* **25**, 1605–1612 (2004).

62. P. Emsley, K. Cowtan, Coot: Model-building tools for molecular graphics. *Acta Crystallogr. D Biol. Crystallogr.* **60**, 2126–2132 (2004).

63. P. D. Adams, P. V. Afonine, G. Bunkóczi, V. B. Chen, I. W. Davis, N. Echols, J. J. Headd, L. W. Hung, G. J. Kapral, R. W. Grosse-Kunstleve, A. J. McCoy, N. W. Moriarty, R. Oeffner, R. J. Read, D. C. Richardson, J. S. Richardson, T. C. Terwilliger, P. H. Zwart, PHENIX: A comprehensive Python-based system for macromolecular structure solution. *Acta Crystallogr. D Biol. Crystallogr.* **66**, 213–221 (2010).

64. E. F. Pettersen, T. D. Goddard, C. C. Huang, E. C. Meng, G. S. Couch, T. I. Croll, J. H. Morris, T. E. Ferrin, UCSF ChimeraX: Structure visualization for researchers, educators, and developers. *Protein Sci.* **30**, 70–82 (2021).

65. Schrodinger, LLC. (2015).

66. M. D. Wilson, S. Benlekbir, A. Fradet-Turcotte, A. Sherker, J. P. Julien, A. McEwan, S. M. Noordermeer, F. Sicheri, J. L. Rubinstein, D. Durocher, The structural basis of modified nucleosome recognition by 53BP1. *Nature* **536**, 100–103 (2016).

67. J. Gao, B. A. Aksoy, U. Dogrusoz, G. Dresdner, B. Gross, S. Onur Sumer, Y. Sun, A. Jacobsen, R. Sinha, E. Larsson, E. Cerami, C. Sander, N. Schultz, Integrative analysis of complex cancer genomics and clinical profiles using the cBioPortal. *Sci. Signal.* **6**, pl1 (2013).

68. E. Cerami, J. Gao, U. Dogrusoz, B. E. Gross, S. Onur Sumer, B. A. Aksoy, A. Jacobsen, C. J. Byrne, M. L. Heuer, E. Larsson, Y. Antipin, B. Reva, A. P. Goldberg, C. Sander, N. Schultz, The cBio cancer genomics portal: An open platform for exploring multidimensional cancer genomics data. *Cancer Discov.* **2**, 401–404 (2012).

69. K. Kim, W. Hu, F. Audenet, N. Almassi, A. J. Hanrahan, K. Murray, A. Bagrodia, N. Wong, T. N. Clinton, S. Dason, V. Mohan, S. Jebiwott, K. Nagar, J. Gao, A. Penson, C. Hughes, B. Gordon, Z. Chen, Y. Dong, P. A. Watson, R. Alvim, A. Elzein, S. P. Gao, E. Cocco, A. D. Santin, I. Ostrovnaya, J. J. Hsieh, I. Sagi, E. J. Pietzak, A. Ari Hakimi, J. E. Rosenberg, G. Iyer, H. A. Vargas, M. Scaltriti,

H. Al-Ahmadie, D. B. Solit, J. A. Coleman, Modeling biological and genetic diversity in upper tract urothelial carcinoma with patient derived xenografts. *Nat. Commun.* **11**, 1975 (2020).

70. J. P. Sfakianos, E. K. Cha, G. Iyer, S. N. Scott, E. C. Zabor, R. H. Shah, Q. Ren, A. Bagrodia, P. H. Kim, A. Ari Hakimi, I. Ostrovnaya, R. Ramirez, A. J. Hanrahan, N. B. Desai, A. Sun, P. Pinciroli, J. E. Rosenberg, G. Dalbagni, N. Schultz, D. F. Bajorin, V. E. Reuter, M. F. Berger, B. H. Bochner, H. A. Al-Ahmadie, D. B. Solit, J. A. Coleman, Genomic characterization of upper tract urothelial carcinoma. *Eur. Urol.* **68**, 970–977 (2015).

71. K. A. Hoadley, C. Yau, T. Hinoue, D. M. Wolf, A. J. Lazar, E. Drill, R. Shen, A. M. Taylor, A. D. Cherniack, V. Thorsson, R. Akbani, R. Bowlby, C. K. Wong, M. Wiznerowicz, F. Sanchez-Vega, A. G. Robertson, B. G. Schneider, M. S. Lawrence, H. Noushmehr, T. M. Malta; Cancer Genome Atlas Network, J. M. Stuart, C. C. Benz, P. W. Laird, Cell-of-origin patterns dominate the molecular classification of 10,000 tumors from 33 types of cancer. *Cell* 1**73**, 291–304.e6 (2018).

72. E. Bernard, H. Tuechler, P. L. Greenberg, R. P. Hasserjian, J. E. Arango Ossa, Y. Nannya, S. M. Devlin, M. Creignou, P. Pinel, L. Monnier, G. Gundem, J. S. Medina-Martinez, D. Domenico, M. Jädersten, U. Germing, G. Sanz, A. A. van de Loosdrecht, O. Kosmider, M. Y. Follo, F. Thol, L. Zamora, R. F. Pinheiro, A. Pellagatti, H. K. Elias, D. Haase, C. Ganster, L. Ades, M. Tobiasson, L. Palomo, M. G. Della Porta, A. Takaori-Kondo, T. Ishikawa, S. Chiba, S. Kasahara, Y. Miyazaki, A. Viale, K. Huberman, P. Fenaux, M. Belickova, M. R. Savona, V. M. Klimek, F. P. S. Santos, J. Boultwood, I. Kotsianidis, V. Santini, F. Solé, U. Platzbecker, M. Heuser, P. Valent, K. Ohyashiki, C. Finelli, M. T. Voso, L.-Y. Shih, M. Fontenay, J. H. Jansen, J. Cervera, N. Gattermann, B. L. Ebert, R. Bejar, L. Malcovati, M. Cazzola, S. Ogawa, E. Hellström-Lindberg, E. Papaemmanuil, Molecular international prognostic scoring system for myelodysplastic syndromes. *NEJM Evidence* **1**, 10.1056/EVIDoa2200008 (2022).

73. A. Zehir, R. Benayed, R. H. Shah, A. Syed, S. Middha, H. R. Kim, P. Srinivasan, J. Gao, D. Chakravarty, S. M. Devlin, M. D. Hellmann, D. A. Barron, A. M. Schram, M. Hameed, S. Dogan, D. S. Ross, J. F. Hechtman, D. F. De Lair, J. J. Yao, D. L. Mandelker, D. T. Cheng, R. Chandramohan, A. S. Mohanty, R. N. Ptashkin, G. Jayakumaran, M. Prasad, M. H. Syed, A. B. Rema, Z. Y. Liu, K. Nafa, L. Borsu, J. Sadowska, J. Casanova, R. Bacares, I. J. Kiecka, A. Razumova, J. B. Son, L.

Stewart, T. Baldi, K. A. Mullaney, H. Al-Ahmadie, E. Vakiani, A. A. Abeshouse, A. V. Penson, P. Jonsson, N. Camacho, M. T. Chang, H. H. Won, B. E. Gross, R. Kundra, Z. J. Heins, H.-W. Chen, S. Phillips, H. Zhang, J. Wang, A. Ochoa, J. Wills, M. Eubank, S. B. Thomas, S. M. Gardos, D. N. Reales, J. Galle, R. Durany, R. Cambria, W. Abida, A. Cercek, D. R. Feldman, M. M. Gounder, A Ari Hakimi, J. J. Harding, G. Iyer, Y. Y. Janjigian, E. J. Jordan, C. M. Kelly, M. A. Lowery, L. G. T. Morris, A. M. Omuro, N. Raj, P. Razavi, A. N. Shoushtari, N. Shukla, T. E. Soumerai, A. M. Varghese, R. Yaeger, J. Coleman, B. Bochner, G. J. Riely, L. B. Saltz, H. I. Scher, P. J. Sabbatini, M. E. Robson, D. S. Klimstra, B. S. Taylor, J. Baselga, N. Schultz, D. M. Hyman, M. E. Arcila, D. B. Solit, M. Ladanyi, M. F. Berger, Mutational landscape of metastatic cancer revealed from prospective clinical sequencing of 10,000 patients. *Nat. Med.* **23**, 703–713 (2017).

74. B. L. Manning-Geist, Y. L. Liu, K. A. Devereaux, A. Da Cruz Paula, Q. C. Zhou, W. Ma, P. Selenica, O. Ceyhan-Birsoy, L. A. Moukarzel, T. Hoang, S. Gordhandas, M. M. Rubinstein, C. F. Friedman, C. Aghajanian, N. R. Abu-Rustum, Z. K. Stadler, J. S. Reis-Filho, A. Iasonos, D. Zamarin, L. H. Ellenson, Y. Lakhman, D. L. Mandelker, B. Weigelt, Microsatellite instability-high endometrial cancers with MLH1 promoter hypermethylation have distinct molecular and clinical profiles. *Clin. Cancer Res.* **28**, 4302–4311 (2022).

75. L. Wu, H. Yao, H. Chen, A. Wang, K. Guo, W. Gou, Y. Yu, X. Li, M. Yao, S. Yuan, F. Pang, J. Hu, L. Chen, W. Liu, J. Yao, S. Zhang, X. Dong, W. Wang, J. Hu, Q. Ling, S. Ding, Y. Wei, Q. Li, W. Cao, S. Wang, Y. Di, F. Feng, G. Zhao, J. Zhang, L. Huang, J. Xu, W. Yan, Z. Tong, D. Jiang, T. Ji, Q. Li, L. Xu, H. He, L. Shang, J. Liu, K. Wang, D. Wu, J. Shen, Y. Liu, T. Zhang, C. Liang, Y. Wang, Y. Shang, J. Guo, G. Liang, S. Xu, J. Liu, K. Wang, M. Wang, Landscape of somatic alterations in large-scale solid tumors from an Asian population. *Nat. Commun.* **13**, 4264 (2022).

76. F. P. Barthel, K. C. Johnson, F. S. Varn, A. D. Moskalik, G. Tanner, E. Kocakavuk, K. J. Anderson, O. Abiola, K. Aldape, K. D. Alfaro, D. Alpar, S. B. Amin, D. M. Ashley, P. Bandopadhayay, J. S. Barnholtz-Sloan, R. Beroukhim, C. Bock, P. K. Brastianos, D. J. Brat, A. R. Brodbelt, A. F. Bruns, K. R. Bulsara, A. Chakrabarty, A. Chakravarti, J. H. Chuang, E. B. Claus, E. J. Cochran, J. Connelly, J. F. Costello, G. Finocchiaro, M. N. Fletcher, P. J. French, H. K. Gan, M. R. Gilbert, P. V. Gould, M. R. Grimmer, A. Iavarone, A. Ismail, M. D. Jenkinson, M. Khasraw, H. Kim, M. C. M. Kouwenhoven, P. S. La Violette, M. Li, P. Lichter, K. L. Ligon, A. K. Lowman, T. M. Malta, T. Mazor, K. L.

McDonald, A. M. Molinaro, D.-H. Nam, N. Nayyar, H. K. Ng, C. Y. Ngan, S. P. Niclou, J. M. Niers, H. Noushmehr, J. Noorbakhsh, D. R. Ormond, C.-K. Park, L. M. Poisson, R. Rabadan, B. Radlwimmer, G. Rao, G. Reifenberger, J. K. Sa, M. Schuster, B. L. Shaw, S. C. Short, P. A. Sillevis Smitt, A. E. Sloan, M. Smits, H. Suzuki, G. Tabatabai, E. G. Van Meir, C. Watts, M. Weller, P. Wesseling, B. A. Westerman, G. Widhalm, A. Woehrer, W. K. A. Yung, G. Zadeh, J. T. Huse, J. F. De Groot, L. F. Stead, R. G. W. Verhaak; The GLASS Consortium, Longitudinal molecular trajectories of diffuse glioma in adults. *Nature* **576**, 112–120 (2019).

77. A. Jusakul, I. Cutcutache, C. H. Yong, J. Q. Lim, M. N. Huang, N. Padmanabhan, V. Nellore, S. Kongpetch, A. W. T. Ng, L. M. Ng, S. P. Choo, S. S. Myint, R. Thanan, S. Nagarajan, W. K. Lim, C. C. Y. Ng, A. Boot, M. Liu, C. K. Ong, V. Rajasegaran, S. Lie, A. S. T. Lim, T. H. Lim, J. Tan, J. L. Loh, J. R. McPherson, N. Khuntikeo, V. Bhudhisawasdi, P. Yongvanit, S. Wongkham, Y. Totoki, H. Nakamura, Y. Arai, S. Yamasaki, P. K.-H. Chow, A. Y. F. Chung, L. L. P. J. Ooi, K. H. Lim, S. Dima, D. G. Duda, I. Popescu, P. Broet, S.-Y. Hsieh, M.-C. Yu, A. Scarpa, J. Lai, D.-X. Luo, A. L. Carvalho, A. L. Vettore, H. Rhee, Y. N. Park, L. B. Alexandrov, R. Gordân, S. G. Rozen, T. Shibata, C. Pairojkul, B. T. Teh, P. Tan, Whole-genome and epigenomic landscapes of etiologically distinct subtypes of cholangiocarcinoma. *Cancer Discov.* **7**, 1116–1135 (2017).

78. A. S. Ho, A. Ochoa, G. Jayakumaran, A. Zehir, C. V. Mayor, J. Tepe, V. Makarov, M. G. Dalin, J. He, M. Bailey, M. Montesion, J. S. Ross, V. A. Miller, L. Chan, I. Ganly, S. Dogan, N. Katabi, P. Tsipouras, P. Ha, N. Agrawal, D. B. Solit, P. A. Futreal, A. K. El Naggar, J. S. Reis-Filho, B. Weigelt, A. L. Ho, N. Schultz, T. A. Chan, L. G. Morris, Genetic hallmarks of recurrent/metastatic adenoid cystic carcinoma. *J. Clin. Invest.* **129**, 4276–4289 (2019).

79. K. Schulze, S. Imbeaud, E. Letouzé, L. B. Alexandrov, J. Calderaro, S. Rebouissou, G. Couchy, C. Meiller, J. Shinde, F. Soysouvanh, A.-L. Calatayud, R. Pinyol, L. Pelletier, C. Balabaud, A. Laurent, J.-F. Blanc, V. Mazzaferro, F. Calvo, A. Villanueva, J.-C. Nault, P. Bioulac-Sage, M. R. Stratton, J. M. Llovet, J. Zucman-Rossi, Exome sequencing of hepatocellular carcinomas identifies new mutational signatures and potential therapeutic targets. *Nat. Genet.* **47**, 505–511 (2015).

80. P. H. Kim, E. K. Cha, J. P. Sfakianos, G. Iyer, E. C. Zabor, S. N. Scott, I. Ostrovnaya, R. Ramirez, A. Sun, R. Shah, A. M. Yee, V. E. Reuter, D. F. Bajorin, J. E. Rosenberg, N. Schultz, M. F. Berger,

H. A. Al-Ahmadie, D. B. Solit, B. H. Bochner, Genomic predictors of survival in patients with high-grade urothelial carcinoma of the bladder. *Eur. Urol.* **67**, 198–201 (2015).

81. J. S. Damrauer, W. Beckabir, J. Klomp, M. Zhou, E. R. Plimack, M. D. Galsky, P. Grivas, N. M. Hahn, P. H. O'Donnell, G. Iyer, D. I. Quinn, B. G. Vincent, D. Z. Quale, S. E. Wobker, K. A. Hoadley, W. Y. Kim, M. I. Milowsky, Collaborative study from the Bladder Cancer Advocacy Network for the genomic analysis of metastatic urothelial cancer. *Nat. Commun.* **13**, 6658 (2022).

82. Y. Sato, T. Yoshizato, Y. Shiraishi, S. Maekawa, Y. Okuno, T. Kamura, T. Shimamura, A. Sato-Otsubo, G. Nagae, H. Suzuki, Y. Nagata, K. Yoshida, A. Kon, Y. Suzuki, K. Chiba, H. Tanaka, A. Niida, A. Fujimoto, T. Tsunoda, T. Morikawa, D. Maeda, H. Kume, S. Sugano, M. Fukayama, H. Aburatani, M. Sanada, S. Miyano, Y. Homma, S. Ogawa, Integrated molecular analysis of clear-cell renal cell carcinoma. *Nat. Genet.* **45**, 860–867 (2013).

83. R. Xue, L. Chen, C. Zhang, M. Fujita, R. Li, S.-M. Yan, C. K. Ong, X. Liao, Q. Gao, S. Sasagawa, Y. Li, J. Wang, H. Guo, Q.-T. Huang, Q. Zhong, J. Tan, L. Qi, W. Gong, Z. Hong, M. Li, J. Zhao, T. Peng, Y. Lu, K. H. T. Lim, A. Boot, A. Ono, K. Chayama, Z. Zhang, S. G. Rozen, B. T. Teh, X. W. Wang, H. Nakagawa, M.-S. Zeng, F. Bai, N. Zhang, Genomic and transcriptomic profiling of combined hepatocellular and intrahepatic cholangiocarcinoma reveals distinct molecular subtypes. *Cancer Cell* **35**, 932–947.e8 (2019).

84. C. Curtis, S. P. Shah, S.-F. Chin, G. Turashvili, O. M. Rueda, M. J. Dunning, D. Speed, A. G. Lynch, S. Samarajiwa, Y. Yuan, S. Gräf, G. Ha, G. Haffari, A. Bashashati, R. Russell, S. M. Kinney; METABRIC Group, A. Langerød, A. Green, E. Provenzano, G. Wishart, S. Pinder, P. Watson, F. Markowetz, L. Murphy, I. Ellis, A. Purushotham, A.-L. Børresen-Dale, J. D. Brenton, S. Tavaré, C. Caldas, S. Aparicio, The genomic and transcriptomic architecture of 2,000 breast tumours reveals novel subgroups. *Nature* **486**, 346–352 (2012).

85. B. Pereira, S.-F. Chin, O. M. Rueda, H.-K. M. Vollan, E. Provenzano, H. A. Bardwell, M. Pugh, L. Jones, R. Russell, S.-J. Sammut, D. W. Y. Tsui, B. Liu, S.-J. Dawson, J. Abraham, H. Northen, J. F. Peden, A. Mukherjee, G. Turashvili, A. R. Green, S. M. Kinney, A. Oloumi, S. Shah, N. Rosenfeld, L. Murphy, D. R. Bentley, I. O. Ellis, A. Purushotham, S. E. Pinder, A.-L. Børresen-Dale, H. M. Earl,

P. D. Pharoah, M. T. Ross, S. Aparicio, C. Caldas, The somatic mutation profiles of 2,433 breast cancers refine their genomic and transcriptomic landscapes. *Nat. Commun.* **7**, 11479 (2016).

86. Y. Y. Li, G. J. Hanna, A. C. Laga, R. I. Haddad, J. H. Lorch, P. S. Hammerman, Genomic analysis of metastatic cutaneous squamous cell carcinoma. *Clin. Cancer Res.* **21**, 1447–1456 (2015).

87. M. Kakiuchi, T. Nishizawa, H. Ueda, K. Gotoh, A. Tanaka, A. Hayashi, S. Yamamoto, K. Tatsuno, H. Katoh, Y. Watanabe, T. Ichimura, T. Ushiku, S. Funahashi, K. Tateishi, I. Wada, N. Shimizu, S. Nomura, K. Koike, Y. Seto, M. Fukayama, H. Aburatani, S. Ishikawa, Recurrent gain-of-function mutations of RHOA in diffuse-type gastric carcinoma. *Nat. Genet.* **46**, 583–587 (2014).

88. F. Petralia, N. Tignor, B. Reva, M. Koptyra, S. Chowdhury, D. Rykunov, A. Krek, W. Ma, Y. Zhu, J. Ji, A. Calinawan, J. R. Whiteaker, A. Colaprico, V. Stathias, T. Omelchenko, X. Song, P. Raman, Y. Guo, M. A. Brown, R. G. Ivey, J. Szpyt, S. G. Thakurta, M. A. Gritsenko, K. K. Weitz, G. Lopez, S. Kalayci, Z. H. Gümüş, S. Yoo, Felipe da Veiga Leprevost, H.-Y. Chang, K. Krug, L. Katsnelson, Y. Wang, J. J. Kennedy, U. J. Voytovich, L. Zhao, K. S. Gaonkar, B. M. Ennis, B. Zhang, V. Baubet, L. Tauhid, J. V. Lilly, J. L. Mason, B. Farrow, N. Young, S. Leary, J. Moon, V. A. Petyuk, J. Nazarian, N. D. Adappa, J. N. Palmer, R. M. Lober, S. Rivero-Hinojosa, L.-B. Wang, J. M. Wang, M. Broberg, R. K. Chu, R. J. Moore, M. E. Monroe, R. Zhao, R. D. Smith, J. Zhu, A. I. Robles, M. Mesri, E. Boja, T. Hiltke, H. Rodriguez, B. Zhang, E. E. Schadt, D R Mani, L. Ding, A. Iavarone, M. Wiznerowicz, S. Schürer, X. S. Chen, A. P. Heath, J. L. Rokita, A. I. Nesvizhskii, D. Fenyö, K. D. Rodland, T. Liu, S. P. Gygi, A. G. Paulovich, A. C. Resnick, P. B. Storm, B. R. Rood, P. Wang; Children's Brain Tumor Network; Clinical Proteomic Tumor Analysis Consortium, Integrated proteogenomic characterization across major histological types of pediatric brain cancer. *Cell* **183**, 1962–1985.e31 (2020).

89. M. Krauthammer, Y. Kong, B. H. Ha, P. Evans, A. Bacchiocchi, J. P. McCusker, E. Cheng, M. J. Davis, G. Goh, M. Choi, S. Ariyan, D. Narayan, K. Dutton-Regester, A. Capatana, E. C. Holman, M. Bosenberg, M. Sznol, H. M. Kluger, D. E. Brash, D. F. Stern, M. A. Materin, R. S. Lo, S. Mane, S. Ma, K. K. Kidd, N. K. Hayward, R. P. Lifton, J. Schlessinger, T. J. Boggon, R. Halaban, Exome sequencing identifies recurrent somatic RAC1 mutations in melanoma. *Nat. Genet.* **44**, 1006–1014 (2012).

90. S. Ren, G.-H. Wei, D. Liu, L. Wang, Y. Hou, S. Zhu, L. Peng, Q. Zhang, Y. Cheng, H. Su, X. Zhou, J. Zhang, F. Li, H. Zheng, Z. Zhao, C. Yin, Z. He, X. Gao, H. E. Zhau, C.-Y. Chu, J. B. Wu, C. Collins, S. V. Volik, R. Bell, J. Huang, K. Wu, D. Xu, D. Ye, Y. Yu, L. Zhu, M. Qiao, H.-M. Lee, Y. Yang, Y. Zhu, X. Shi, R. Chen, Y. Wang, W. Xu, Y. Cheng, C. Xu, X. Gao, T. Zhou, B. Yang, J. Hou, L. Liu, Z. Zhang, Y. Zhu, C. Qin, P. Shao, J. Pang, L. W. K. Chung, J. Xu, C.-L. Wu, W. Zhong, X. Xu, Y. Li, X. Zhang, J. Wang, H. Yang, J. Wang, H. Huang, Y. Sun, Whole-genome and transcriptome sequencing of prostate cancer identify new genetic alterations driving disease progression. *Eur. Urol.* **73**, 322–339 (2018).

91. E. Pleasance, E. Titmuss, L. Williamson, H. Kwan, L. Culibrk, E. Y. Zhao, K. Dixon, K. Fan, R. Bowlby, M. R. Jones, Y. Shen, J. K. Grewal, J. Ashkani, K. Wee, C. J. Grisdale, M. L. Thibodeau, Z. Bozoky, H. Pearson, E. Majounie, T. Vira, R. Shenwai, K. L. Mungall, E. Chuah, A. Davies, M. Warren, C. Reisle, M. Bonakdar, G. A. Taylor, V. Csizmok, S. K. Chan, Z. Zong, S. Bilobram, A. Muhammadzadeh, D. D'Souza, R. D. Corbett, D. M. Millan, M. Carreira, C. Choo, D. Bleile, S. Sadeghi, W. Zhang, T. Wong, D. Cheng, S. D. Brown, R. A. Holt, R. A. Moore, A. J. Mungall, Y. Zhao, J. Nelson, A. Fok, Y. Ma, M. K. C. Lee, J.-M. Lavoie, S. Mendis, J. M. Karasinska, B. Deol, A. Fisic, D. F. Schaeffer, S. Yip, K. Schrader, D. A. Regier, D. Weymann, S. Chia, K. Gelmon, A. Tinker, S. Sun, H. Lim, D. J. Renouf, J. Laskin, S. J. M. Jones, M. A. Marra, Pan-cancer analysis of advanced patient tumors reveals interactions between therapy and genomic landscapes. *Nat. Cancer* **1**, 452–468 (2020).

92. G. Guo, J. Chmielecki, C. Goparaju, A. Heguy, I. Dolgalev, M. Carbone, S. Seepo, M. Meyerson, H. I. Pass, Whole-exome sequencing reveals frequent genetic alterations in BAP1, NF2, CDKN2A, and CUL1 in malignant pleural mesothelioma. *Cancer Res.* **75**, 264–269 (2015).

93. D. M. Hyman, S. A. Piha-Paul, H. Won, J. Rodon, C. Saura, G. I. Shapiro, D. Juric, D. I. Quinn, V. Moreno, B. Doger, I. A. Mayer, V. Boni, E. Calvo, S. Loi, A. C. Lockhart, J. P. Erinjeri, M. Scaltriti, G. A. Ulaner, J. Patel, J. Tang, H. Beer, S. D. Selcuklu, A. J. Hanrahan, N. Bouvier, M. Melcer, R. Murali, A. M. Schram, L. M. Smyth, K. Jhaveri, B. T. Li, A. Drilon, J. J. Harding, G. Iyer, B. S. Taylor, M. F. Berger, R. E. Cutler Jr., F. Xu, A. Butturini, L. D. Eli, G. Mann, C. Farrell, A. S. Lalani, R. P. Bryce, C. L. Arteaga, F. Meric-Bernstam, J. Baselga, D. B. Solit, HER kinase inhibition in patients with HER2- and HER3-mutant cancers. *Nature* **554**, 189–194 (2018).

94. The ICGC/TCGA Pan-Cancer Analysis of Whole Genomes Consortium, Pan-cancer analysis of whole genomes. *Nature* **578**, 82–93 (2020).

95. D. Miao, C. A. Margolis, W. Gao, M. H. Voss, W. Li, D. J. Martini, C. Norton, D. Bossé, S. M. Wankowicz, D. Cullen, C. Horak, M. Wind-Rotolo, A. Tracy, M. Giannakis, F. S. Hodi, C. G. Drake, M. W. Ball, M. E. Allaf, A. Snyder, M. D. Hellmann, T. Ho, R. J. Motzer, S. Signoretti, W. G. Kaelin Jr., T. K. Choueiri, E. M. Van Allen, Genomic correlates of response to immune checkpoint therapies in clear cell renal cell carcinoma. *Science* **359**, 801–806 (2018).

96. P. Johansson, L. G. Aoude, K. Wadt, W. J. Glasson, S. K. Warrier, A. W. Hewitt, J. F. Kiilgaard, S. Heegaard, T. Isaacs, M. Franchina, C. Ingvar, T. Vermeulen, K. J. Whitehead, C. W. Schmidt, J. M. Palmer, J. Symmons, A.-M. Gerdes, G. Jönsson, N. K. Hayward, Deep sequencing of uveal melanoma identifies a recurrent mutation in *PLCB4*. *Oncotarget* **7**, 4624–4631 (2016).

97. S. Vasaikar, C. Huang, X. Wang, V. A. Petyuk, S. R. Savage, B. Wen, Y. Dou, Y. Zhang, Z. Shi, O. A. Arshad, M. A. Gritsenko, L. J. Zimmerman, J. E. McDermott, T. R. Clauss, R. J. Moore, R. Zhao, M. E. Monroe, Y.-T. Wang, M. C. Chambers, R. J. C. Slebos, K. S. Lau, Q. Mo, L. Ding, M. Ellis, M. Thiagarajan, C. R. Kinsinger, H. Rodriguez, R. D. Smith, K. D. Rodland, D. C. Liebler, T. Liu, B. Zhang; Clinical Proteomic Tumor Analysis Consortium, Proteogenomic analysis of human colon cancer reveals new therapeutic opportunities. *Cell* **177**, 1035–1049.e19 (2019).

98. M. Jamal-Hanjani, G. A. Wilson, N. M. Granahan, N. J. Birkbak, T. B. K. Watkins, S. Veeriah, S. Shafi, D. H. Johnson, R. Mitter, R. Rosenthal, M. Salm, S. Horswell, M. Escudero, N. Matthews, A. Rowan, T. Chambers, D. A. Moore, S. Turajlic, H. Xu, S.-M. Lee, M. D. Forster, T. Ahmad, C. T. Hiley, C. Abbosh, M. Falzon, E. Borg, T. Marafioti, D. Lawrence, M. Hayward, S. Kolvekar, N. Panagiotopoulos, S. M. Janes, R. Thakrar, A. Ahmed, F. Blackhall, Y. Summers, R. Shah, L. Joseph, A. M. Quinn, P. A. Crosbie, B. Naidu, G. Middleton, G. Langman, S. Trotter, M. Nicolson, H. Remmen, K. Kerr, M. Chetty, L. Gomersall, D. A. Fennell, A. Nakas, S. Rathinam, G. Anand, S. Khan, P. Russell, V. Ezhil, B. Ismail, M. Irvin-Sellers, V. Prakash, J. F. Lester, M. Kornaszewska, R. Attanoos, H. Adams, H. Davies, S. Dentro, P. Taniere, B. O'Sullivan, H. L. Lowe, J. A. Hartley, N. Iles, H. Bell, Y. Ngai, J. A. Shaw, J. Herrero, Z. Szallasi, R. F. Schwarz, A. Stewart, S. A. Quezada,

J. L. Quesne, P. Van Loo, C. Dive, A. Hackshaw, C. Swanton; TRACERx Consortium, Tracking the evolution of non-small-cell lung cancer. *N. Engl. J. Med.* **376**, 2109–2121 (2017).